UNIVERSITY OF CALIFORNIA,
IRVINE

Pursuit and Evasion Strategies in Zebrafish: Mathematical Modeling and Behavioral Experiments

DISSERTATION

submitted in partial satisfaction of the requirements
for the degree of

DOCTOR OF PHILOSOPHY

in Biological Sciences

by

Alberto Prado Soto

Dissertation Committee:
Professor Matthew J. McHenry, Chair
Professor Timothy J. Bradley
Associate Professor Manny Azizi

2019

DEDICATION

Para mis queridos padres,
Agustin Viramontes Soto q.e.p.d. y Paulina Nava Soto,
que me han dado la oportunidad de estudiar y realizar este logro intelectual.

To my siblings,
Carlos y Magdalena Soto,
'I'm little bro and big bro all at once – Promise I am never letting up'

To my lovely wife,
Hilda Prado Soto,
this dissertation would not have been possible without your
generous patience, unwavering support, and invaluable feedback.

Para mi hijo,
Benny Alessandro Soto,
you have been the ultimate driver of my academic pursuits.
In the near future, I may even have a real job you can be proud of.

TABLE OF CONTENTS

LIST OF FIGURES

ACKNOWLEDGMENTS

I am very grateful to have had Dr. Matt McHenry as my dissertation advisor. He treated me like a colleague since I started working in his lab and has provided invaluable support throughout my graduate tenure. The contents of this dissertation reflect my diverse scientific interests, which I wouldn't have been able to explore without Dr. McHenry's open mind.

A special thanks to members of the Comparative Physiology Group at UC Irvine. 210 has provided training and professional development that few students in doctoral programs receive. In particular, I would like to thank the intellectual contributions of my committee members Dr. Tim Bradley and Dr. Manny Azizi. They have supported and advanced my research through challenging questions and insightful knowledge of physiology and biomechanics.

The McHenry Lab has been an exceptional fit for my doctoral work. The interdisciplinary nature of our work benefits from having members with diverse backgrounds and interests. The fact that many of my lab mates are incredibly skilled cooks and bakers made for a more delightful and delicious grad school exprience.

SACNAS at UCI deserves a special acknowledgement. Underrepresented minorities in STEM face unique challenges in pursuing higher education. We are forced to navigate an incredibly perplexing academic landscape that often ignores our unique cultures and undervalues our work. It is through organizations such as SACNAS that we make progress, change the face of science, and truly diversify the scientific workforce of the United States.

I thank Oxford University Press and the Company of Biologists Ltd. for permission to include copyrighted material as part of my thesis/dissertation. Financial support was provided by the University of California, Irvine, the NSF Graduate Research Fellowship Program (DGE-1839285), NIH training grant (T32-HD060555) awarded to Arthur Lander, NSF grant (IOS-1354842) awarded to MJ McHenry, and ONR grants (N00014-15-1-2249 and N00014-19-1-2035) awarded to MJ McHenry.

CURRICULUM VITAE

Alberto Prado Soto

Education

2019 **Ph.D. in Biological Sciences**
University of California, Irvine, CA.
Advisor: Dr. Matt McHenry
Concentration: Ecology & Evolutionary Biology

2014 **M.S. in Mathematics**
University of California, Irvine, CA.

2012 **B.S. in Applied Mathematics**
California State Polytechnic University, Pomona, CA.
cum laude

Publications

Soto, A.P., Po, T., McHenry, M.J. Multichannel Stroboscopic Videography (MSV): A technique for visualizing multiple channels for behavioral measurements. Journal of Experimental Biology. May 2019 (in press)

McHenry, M.J., Johansen, J.L., **Soto, A.P.**, Free, B.A., Paley, D.A., Liao, J.C. The pursuit strategy of predatory bluefish (*Pomatomus saltatrix*). 286. Proceedings of the Royal Society B: Biological Sciences. Feb. 2019; doi:10.1098/rspb.2018.2934

Soto, A., Stewart, W.J., McHenry, M.J. When optimal strategy matters to prey fish. Integrative and Comparative Biology. July 2015; doi:10.1093/icb/icv027.

Honors and Awards

2019 **Grover Stephens Memorial Fellowship**
School of Biological Sciences, UC Irvine.

2019 **Graduate Student Excellence Award**
Latino Excellence and Achievement Dinner, UC Irvine.

2019 **SICB Broadening Participation Travel Grant**
Society for Integrative and Comparative Biology, Tampa, FL

2018 **ComSciCon Travel Fellowship**
ComSciCon, Boston, MA.

2017 **SICB Broadening Participation Travel Grant**
Society for Integrative and Comparative Biology, New Orleans, LA

2015 **Friday Harbor Labs Wainwright Fellowship**
University of Washington, Friday Harbor Labs.

2015 **Best Student Oral Presentation**
Southwest Organismal Biology Regional Conference, Cal Poly Pomona.

2014 **NSF Graduate Research Fellowship Program**
National Science Foundation.

2013 **CCBS Predoctoral Training Grant**
National Institute of Biomedical Imaging and Bioengineering –
from UC Irvine, Center for Complex Biological Systems.

2013 **Graduate MBRS Scholar**
Minority Biomedical Research Support Program for Graduates,
School of Biological Sciences, UC Irvine.

2012 **SACNAS Annual Meeting Travel Award (Seattle, WA)**
SACNAS, Inc., Santa Cruz, CA.

2012 **Best Poster Presentation**
SIAM Life Sciences Conference, San Diego, CA.

2012 **President's List**
California State Polytechnic University, Pomona, CA.

2012 **Dean's List**
California State Polytechnic University, Pomona, CA.

2011 **SACNAS Annual Meeting Travel Award (Fresno, CA)**
SACNAS, Inc., Santa Cruz, CA.

2011 **North Carolina State University REU (NSF Funded)**
North Carolina State University, Raleigh, NC.

2011 **Building Diversity in Science Scholarship**
Building Diversity in Science, Inc., Daly City, CA.

2011 **The Boeing Company Mathematics Department Scholarship**
California State Polytechnic University, Pomona, CA.

Conference Activity

2019 "The hydrodynamics and control of prey pursuit in zebrafish." Oral presentation at

the SICB Annual Meeting in Tampa, FL.

2017 "Prey targeting with intermittent locomotion in zebrafish." Oral presentation at the SICB Annual Meeting in New Orleans, LA.

2016 "The pursuit strategy of predatory zebrafish." Poster presentation at the SICB Annual Meeting in Portland, OR.

2015 SACNAS Annual Meeting, Washington DC.

2015 "Optimal escape directions in predator–prey interactions." Oral presentation at the Southwest Organismal Biology Regional Conference at Cal Poly Pomona.

2015 "Modeling the optimal evasion strategy of prey fish." Poster presentation at the SICB Annual Meeting in West Palm Beach, FL.

2014 SACNAS Annual Meeting, Los Angeles, CA.

2014 SICB Annual Meeting, Austin, TX (Jan 3–7).

2013 SIAM Annual Meeting, San Diego, CA.

2013 Joint Mathematics Meetings, San Diego, CA.

2012 "Modeling Blood Pressure Dynamics." Poster Session at the Society for Industrial and Applied Mathematics Life Sciences Conference in San Diego, CA.

2012 "Modeling Blood Pressure Dynamics." Oral presentation at the Pacific Coast Undergraduate Mathematics Conference at Cal Poly Pomona, CA.

2012 SACNAS Annual Meeting, Seattle, WA.

2012 "Modeling Blood Pressure Dynamics." Poster Session at the Joint Mathematics Meetings in Boston, MA.

2011 SACNAS Annual Meeting, San Jose, CA.

Professional Membership

American Mathematical Society, Society for Industrial and Applied Mathematics, Society for Advancement of Chicanos and Native Americans in Science, Society for Integrative and Comparative Biology.

Service and Outreach

Science Policy Advocate, Coalition for National Science Funding (May. 2018). Participated in the CNSF Capitol Hill Day 2018 on behalf of UC Irvine graduate students. Met with Congressional staff members to advocate for increased NSF funding. Discussed importance of training and mentoring programs for underrepresented minority students.

Co-Founder and Treasurer, SACNAS at UCI (2017-2019). Co-founded the SACNAS graduate student chapter at UC Irvine. Led successful fundraising efforts for the organiza-

tion. Received Best Educational Outreach Program at the Anteater Awards 2019.
Loh Down Script Writer, Loh Down on Science Podcast (2016-2018). Wrote twenty scripts for Sandra Tsing Loh's 'Loh Down on Science' Podcast. Peer edited forty scripts from fellow writer.
Mentoring Across Differences Presenter, Mentoring Excellence Program at UC Irvine (2016-2017). Co-led a workshop on mentoring diverse populations. Workshop attended by UCI graduate students and post-docs.
MSP Symposium Poster Judge, UCI (Sept. 2016). Participated in the Minority Science Program Summer Symposium as a judge during the poster session.
SURF Peer Mentor, UCI (Summer 2016). Participated in the Summer Undergraduate Research Fellowship program as a peer mentor. I assisted students in preparing their poster presentations.
Competitive Edge Peer Mentor, UCI (Summer 2014-2018). Graduate student peer mentor for incoming minority graduate students participating in the Competitive Edge Summer Research Program as part of the DECADE initiative. I served as the peer mentor for two students entering the Dept. of Ecology and Evolutionary Biology.
Graduate Student Recruiter, UCI (Fall 2014-2016). Graduate student recruiter representing UCI at the SACNAS Annual Meeting. I worked alongside Dr. Frances Leslie, Dean of Graduate Studies, and Daniel Fabrega, recruitment manager, at the informational booth for UCI. Hundreds of prospective graduate students from underrepresented minority groups visit the booth at SACNAS.
REU Workshop Panelist, UCI (Nov. 2014-2015). Participated as a panelist in an informational workshop hosted by graduate students in the Department of Ecology and Evolutionary Biology. The workshop topic was NSF funded REUs and was geared toward undergraduate students.
Competitive Edge Peer Mentor, UCI (Summer 2014). Graduate student peer mentor for incoming minority graduate students participating in the Competitive Edge Summer Research Program as part of the DECADE initiative. I served as the peer mentor for two students entering the Dept. of Mathematics.
MCB Bootcamp tutor, UCI (Aug. 2014). Mathematics tutor for incoming Mathematical and Computational Biology PhD Program students during Bootcamp.
COSMOS Teaching Assistant, UCI (Summer 2014). Mathematics tutor for high school students conducting summer research at UCI on cancer tumor modeling through COSMOS.
MCB Bootcamp tutor, UCI (Aug. 2013-2015). Mathematics tutor for incoming Mathematical and Computational Biology PhD Program students during Bootcamp.
MCBU tutor, UCI (July 2013). Mathematics tutor for Mathematical and Computational Biology for Undergraduates summer research experience. Paired teams of mathematics and biology students are co–advised by mathematics and biology faculty.
AVID Program, UCI (April 2013). Research talk to Ontario High School AVID students hosted by the Minority Science Program.
MCB recruits research seminar, UCI (Feb. 2013). Research seminar for Mathematical and Computational Biology PhD Program recruits.
AfterMath Conference Panelist, Harvey Mudd College (Feb. 2013). I was a panelist during the Graduate School Panel at the AfterMath Conference: Preparing for Careers in

the Mathematical Sciences.
Private tutor, (2009–2012). Tutored middle school and high school students in algebra, geometry, and calculus.

ABSTRACT OF THE DISSERTATION

Pursuit and Evasion Strategies in Zebrafish: Mathematical Modeling and Behavioral Experiments

By

Alberto Prado Soto

Doctor of Philosophy in Biological Sciences

University of California, Irvine, 2019

Professor Matthew J. McHenry, Chair

Predator-prey interactions are important to the ecology and evolution of animals and have major implications for the behavioral and locomotor strategies they exhibit. They offer a system to study the strategies used by animals to pursue prey and evade predators from both a theoretical and experimental perspective. Here I have mathematically modeled the evasion strategy of prey fish, conducted experiments to assess the pursuit strategy of zebrafish, and developed a technique to investigate the biomechanics of fish locomotion during pursuit.

My first dissertation chapter revisited the mathematics of a classic pursuit-evasion model and tested the predictions against empirical data on the escape response of larval zebrafish. The evasion strategy of prey in response to an approaching predator had been previously modeled and predicted an optimal escape direction based on the relative speed of the prey, but empirical results often failed to confirm the model predictions. I revisited and generalized the model to reveal a large region of parameter space that predicted a previously unknown performance plateau. The plateau indicated that fast prey can escape away from a slower predator in many directions without diminishing their escape performance. I tested

the model predictions against data on the escape direction of larval zebrafish in response to an approaching robotic predator and found general agreement.

Chapter two of my dissertation focused on the pursuit strategy of zebrafish in pursuit of prey. To study the locomotion of zebrafish chasing prey, I built an experimental setup to film predator–prey interactions at high–speed. These interactions were automatically analyzed with a custom image processing algorithm that tracks the midline of the predator and the position of the prey through time. I confirmed that zebrafish swim intermittently in a burst–and–coast swimming pattern during pursuit. The predator turned and accelerated toward the prey with a single tail beat. The change in heading during a turning maneuver could be predicted by the bearing angle immediately before the burst phase and was correlated with the lateral excursion of the caudal fin. This intermittent pursuit strategy is a form of pure pursuit in which the predator aligns its heading with the position of the prey.

My third dissertation chapter developed a technique to acquire multichannel imaging data using a single camera. In chapter two, I found that zebrafish predators execute turning maneuvers that orient them toward the position of the prey. A mechanistic understanding of how fish execute turning maneuvers continues to elude biologists and physicists alike because it requires measuring the forces produced by the swimming fish. I addressed this challenge by designing an experimental system which allows for simultaneous acquisition of images for flow visualization and automatic tracking using a single high–speed video camera. This technique, Multichannel Stroboscopic Videography (MSV), provides the ability to automate measurements of both the animal's body and flow field and illustrates MSV's powerful capacity for high-throughput experimentation with a complex hydrodynamic analysis.

Introduction

Organisms need to eat and avoid being eaten to survive. These two challenges have major implications for the behavioral and locomotor strategies they exhibit. Many fishes are subject to predation throughout their life and are predators themselves. Zebrafish are a small freshwater species (Family Cyprinidae) of fish native to rivers and inland streams of India (Parichy, 2015). They are omnivores and begin actively hunting for food at 5 days post fertilization (dpf). In the wild, they also have to contend with predation by other fish such as the knifefish (*Notopterus)* (Parichy, 2015). In the lab, juvenile and adult zebrafish will readily prey on larvae of the same species. This makes it tractable to study their behavior and locomotion as predator and prey at the same time, depending on the fish's life stage. The goal of this dissertation is to address the locomotor strategies that fish implement to pursue prey and evade predators. I begin by offering a brief introduction to predator-prey interactions and describe how an interdisciplinary approach enables the synthesis of complex animal behavior.

The violent encounters between predator and prey have long fascinated humans and they have been an exciting topic of inquiry for biologists. Animals have acquired a large variety of specialized mechanisms and tactics for prey capture (e.g. Catania, 2009; deVries et al., 2012; Domenici et al., 2000) and predator evasion (e.g., Emlen, 2014; Evans and Schmidt, 1990). Given the wide range of tactics observed in nature, mathematical modeling coupled

with traditional experimental approaches is increasingly becoming an attractive method for understanding animal behavior during predator-prey interactions (Lima and Dill, 2011; Morice et al., 2013; Brighton et al., 2017). Despite the large number of experimental studies describing the kinematics of escape maneuvers and predatory strikes, a concise theoretical framework for understanding the optimal strategies remains unresolved. The purpose of this introduction is to describe the mathematical and experimental tools available to biologists interested in understanding the strategies employed by organisms during predator-prey interactions. I begin with a brief description of experimental studies that have advanced our mechanistic understanding of predator-prey interactions. Then I discuss the mathematics of optimal strategies and detail a classic model that can be applied to study evasion strategy (Weihs and Webb, 1984). In the last section I describe two pursuit strategies commonly found in nature.

Predator-prey interactions in the lab

Predator-prey interactions vary across animal groups and by environment. For example, an animal's habitat is known to affect both locomotor performance (McElroy et al., 2007; Vanhooydonck and Van Damme, 2003) and predator evasion strategy (Morice et al., 2013; Vasquez et al., 2002). Experimental studies of predator-prey interactions are often restricted to laboratory settings and typically only consider the strategy of either the predator or the prey (Lima, 2002). Despite the limited scope of these studies, they can reveal the strategies used by animals to escape predators (e.g., Card and Dickinson, 2008; Casas and Steinmann, 2014) or pursue prey (e.g., Ghose et al., 2006; McHenry et al., 2019). These studies also provide rich datasets that can be used to test the predictions of mathematical models (see chapter 1). Here, I briefly describe one such approach that uses a model predator to investigate the evasion strategy of prey.

Using model predators to study prey escape strategy

Simultaneously considering predator and prey actions during a predatory interaction is a difficult problem from both an experimental and a theoretical perspective. For this reason, many experimental studies on predator evasion have focused solely on the actions of the prey (Lima, 2002). This is typically achieved by presenting an artificial stimulus to elicit an escape response (reviewed by Domenici and Blagburn, 2011a,b). An artificial stimulus reduces the complexity of the interaction and allows the experimenter to control important aspects of the interaction, such as the direction and speed of the approach. While these qualities often make experiments tractable, an artificial stimulus may not provide appropriate sensory stimuli for prey. Model predators offer an alternative to this approach by presenting a mimic of a natural predator, which is of greater ecological relevance, while also controlling the kinematics of an attack. This approach has been used to study predator evasion in fish (Stewart et al., 2014) and birds (Kullberg et al., 1998).

Larval zebrafish (*Danio rerio*) use their lateral line system to detect subtle water disturbances generated by an approaching predator (Stewart et al., 2013). This allows prey to detect the bow wave generated by the motion of a predator and to direct their escape away from the side of the body that perceives higher flow rates (Stewart et al., 2014). The robotic predator described in (Stewart et al., 2014) controls for the trajectory of an attack and thus allows for the investigation of prey evasion strategy under varying conditions such as predator approach speed. Using a similar experimental approach, male great tits (*Parus major*) have been shown to vary their takeoff (escape) angle in response to the approach direction of a model predator (Kullberg et al., 1998). Although these examples fix the predator strategy, they have provided insight into how prey respond to specific predatory threats. Mathematical modeling can then be used to determine whether or not prey are performing optimally.

Mathematics of optimal strategy

The mathematics of decision-making in conflict situations is grounded in game theory (Aliprantis and Chakrabarti, 2011). Classic game theory deals with what are known as static games (Gibbons, 1992). For example, the game of chess is a static game as moves are made one after the other and there are a finite number of possible moves. There are many situations in which decisions are made dynamically and the number of possible moves is not finite. A classic example is that of a missile interceptor, which must track its target in real-time and correct its trajectory toward the target by implementing a programmed pursuit strategy. This is an example of dynamic games, which were introduced by Rufus Isaacs in the 1950's in a series of RAND Corporation reports.

Differential game theory and pursuit-evasion games

Differential game theory (Isaacs, 1965) combines elements of game theory (strategy) and optimal control theory (optimization) to study the optimal strategies during interactions, or games, between two or more players. The theory has applications in areas as diverse as biology (Alpern et al., 2011), military combat (Jarmark et al., 1981), and robotics (Karaman and Frazzoli, 2011b). For the purpose of this introduction, I will focus on a particular class of problems known as pursuit-evasion games that have direct applications in biology.

Pursuit-evasion (PE) games deal with the problem of a pursuer attempting to capture an evader, such as a cheetah chasing down a gazelle. Associated with any game is a numerical quantity which the pursuer attempts to minimize and the evader attempts to maximize. This quantity is called the *payoff*. In a PE game where capture is the objective, it is mathematically convenient to consider the time of capture as the payoff. Note that within

this setting, the goal of the pursuer is to capture the evader in the least amount of time while the evader attempts to hold off capture as long as possible or indefinitely (infinite time would indicate successful escape). The solution to a game, the so-called minimax solution, includes a set of optimal strategies, one each for the pursuer and evader, which yields the greatest minimal payoff (minimax payoff). This implies a precarious scenario in which any deviation from the optimal strategy by the pursuer leads to a better payoff for the evader and vice versa. Rigorous solutions to even the simplest games are very complex and thus the theory has not been widely applied to biological systems. Advances in numerical techniques for solving differential games (e.g., Bardi et al., 1999; Karaman and Frazzoli, 2011a) provide important tools for researchers interested in applying this theory to biological systems, but these methods are beyond the scope of this dissertation. Another approach to making problems tractable is to make modeling assumptions that can be justified by appealing to biomechanical constraints of the biological system in question (Justh and Krishnaprasad, 2006). This is analogous to fixing the predator strategy by using a model predator in experiments (as described in the previous section).

A biological application of differential game theory

The homicidal chauffeur is the macabre title for a pursuit-evasion game (Isaacs, 1965) that has been adapted to model predator-prey interactions (Weihs and Webb, 1984; Ghose et al., 2006). In this game a driver (the pursuer) attempts to run-down a more agile pedestrian (the evader) in a large parking lot. Although the full analytical solution to this game is complex and multivalued (Merz, 1971), a reduced version can be solved by geometric arguments. To determine the optimal escape direction a prey should travel when attacked by a predator, Weihs and Webb adapted the homicidal chauffeur game. In chapter 1 of this dissertation, I discuss the Weihs and Webb model in detail and offer a new interpretation of their results based on measurements of escape direction in larval zebrafish.

Pursuit strategy

A pursuit strategy defines how the pursuer maneuvers toward the evader during pursuit-evasion games. From a biological perspective, they can be interpreted as the behavioral algorithms implemented by predators targeting evasive prey. Predators in pursuit of evasive prey have to redirect their motion in response to the prey's actions. Theoretically, there exist many possible solutions to this problem (Nahin, 2007). Here I focus on two fundamental pursuit strategies found in nature, pure pursuit and interception.

Pure pursuit is a form of targeting in which the pursuer (or predator) aligns its direction of travel with the instantaneous position of the evader. The typical trajectory traced by a predator implementing pure pursuit against a nonevasive prey is curvilinear (see Chapter 2 Fig. 2.1). If the predator is faster than the prey, then it is guaranteed capture given sufficient time. This pursuit strategy is implemented, for example, by houseflies (Land and Collett, 1974) and bats (Chiu et al., 2010) pursuing conspecifics, and tiger beetles pursuing prey dummies (Gilbert, 1997). When vision is the dominant sensory modality during pursuit behavior, the position of the prey on the predator's retina is sufficient information to implement pure pursuit. For this reason, pure pursuit is often characterized as a simple strategy; although, it requires continuous sensory feedback.

Interception requires that the pursuer compute a pursuit path that will coincide with the evader's estimated future position. The pursuit path must take into account the relative speed and heading of the evader at the onset of a pursuit. The trajectory traced by a predator on an interception path against nonevasive prey is a straight line (see Chapter 2 Fig. 2.1). Compared with pure pursuit, this strategy is time optimal under certain assumptions (Justh and Krishnaprasad, 2006). Interception is used by hoverflies (Collett and Land, 1978) and dragonflies pursuing nonevasive prey dummies (Olberg et al., 2007). Evasive prey maneuvers during pursuit require the computation of a new interception path,

as exhibited by bats in pursuit of evasive moths (Ghose et al., 2006) and goshawks flying toward targets or pursuing prey (Kane et al., 2015). This strategy is known as constant absolute target direction and is equivalent to interception for evasive prey. Interception is thought to be an open-loop behavior, once a pursuit path is computed the pursuer must commit (Moore and Biewener, 2015), but a different interpretation based on visual fixation suggests that predators can implement this strategy without computing an interception path (Olberg et al., 2000).

The current dissertation

The three chapters that comprise this dissertation underscore the value of combining mathematical modeling with behavioral experiments to study complex animal behavior. In chapter one, I have shown that a simplified pursuit-evasion model generates testable hypotheses about escape strategy. In chapter two, I resolved the pursuit strategy of an intermittent swimmer and developed methods for modeling active pursuit in fish. In chapter three, I developed a technique to acquire multichannel data using a single camera that may be applied to study the biomechanics of fish maneuvers, which was a critical component of the pursuit strategy found in chapter two.

Chapter 1

When Optimal Strategy Matters to Prey Fish

1.1 Abstract

Predator-prey interactions are commonly studied with an interest in determining whether prey adopt an optimal strategy to evade predators. Here we examine the strategic consequences of deviating from optimal strategy in fish that are preyed upon by fish predators. We simulated these interactions with numerical and analytical mathematics and compared our predictions with measurements in zebrafish (*Danio rerio*). As in previous models, we focused on the effect of the escape direction on the minimum distance between predator and prey. We found that differences in escape direction had only a small effect on the minimum distance when predators were more than an order of magnitude faster than the prey. Furthermore, differences in direction had no effect on performance for a broad range of escape angles when the prey were faster than the predator. Optimal strategy is therefore most meaningful to prey when approached by a predator of intermediate speed. When the

predator is either slower or much faster than the prey, an optimal strategy may not exist or offer little benefit to predator evasion.

1.2 Background

Biologists have long–appreciated the importance of predation in the ecology and evolution of prey species. This subject is extensive enough to fill the pages of books with the fascinating diversity of strategies that prey use to avoid encounters with predators (e.g. Ruxton et al., 2004) or to defend themselves when discovered (e.g. Emlen, 2014; Evans and Schmidt, 1990). In contrast, our understanding for how prey evade capture by locomotion is relatively rudimentary. Although biomechanical studies commonly speculate on the importance of locomotor performance to survival, relatively few have tested what aspects of locomotion are most meaningful in these interactions. Studies that have explored this subject (reviewed by Domenici and Blagburn, 2011a) underscore the common-sense notion that the direction of an escape matters to a prey's survival. This idea is formalized by pursuit models that aim to determine the optimal direction of an escape response. The present study examined such a model, based on Weihs and Webb (1984), to consider the strategic consequences of deviating from optimal strategy in piscivorous interactions. We compared the model's predictions to experimental results in zebrafish (*Danio rerio*) (Stewart et al., 2014) and arrived at new interpretations of theory on prey strategy.

Pursuit–evasion models are an area of differential game theory that offers a basis for examining locomotor behavior in strategic terms. There is recent interest in revisiting these models (e.g. Howland, 1974; Weihs and Webb, 1984) with experimental studies that consider the behavior of both predators and prey. This includes work on running vertebrates (e.g. Wilson et al., 2013), birds (e.g. Kullberg et al., 1998) and bats (e.g. Ghose et al., 2006) in flight, running insects (Domenici et al., 2008), flying insects (e.g. Combes et al., 2012),

and swimming zooplankton (e.g. Arnott et al., 1999; Heuch et al., 2007) and fishes (e.g. Domenici et al., 2000). These efforts offer the potential to reveal how sensory and motor systems govern the outcome of predator–prey interactions.

A piscivorous interaction offers some advantages as a model for examining the sensory-motor basis of predator evasion. In many cases, this interaction can be easily studied in a laboratory, where predatory fishes attempt to feed on prey and prey initiate a 'fast-start' escape response (Fig. 1.1). Both players operate with motion that is largely two-dimensional and therefore relatively simple to measure and describe. Zebrafish adults prey on larvae of the same species in the lab (Stewart et al., 2013) and this species offers a growing wealth of understanding in physiology and neuroscience (e.g. McLean and Fetcho, 2011; Briggs, 2002) that may be leveraged for mechanistic insight on predator–prey interactions. In addition, fish offer one of the few biological pursuit systems that have been mathematically modeled (Weihs and Webb, 1984). This model offers specific predictions of swimming trajectories that may be tested with kinematic measurements.

Deviation from optimal strategy has been interpreted as a strategic adaptation. The protean hypothesis suggests that prey that are unpredictable have an advantage in predator evasion over predictable prey (Humphries and Driver, 1970). This idea may apply to the erratic motion of an individual or a population of prey that collectively exhibit variable motion that challenges a predator's ability to learn or adapt. The fast start of a fish generates a turn and acceleration of the body in a particular direction and therefore would appear to correspond to the latter category (Weihs, 1973). Regardless, a potential trade-off exists between a direction that generates optimal displacement from a predator and one that is unpredictable.

Interpretations of prey motion have generally not considered the implications of deviating from optimal strategy. For example, it is not clear whether an escape that is $5\,^\circ$ or $50\,^\circ$ from

the optimum predicted by Weihs and Webb (1984) has a major or negligible effect on evasion success. If the performance of an escape is insensitive to differences in escape direction, then no trade-off will exist between evasiveness and predictability. In short, it is unclear when optimal strategy matters. The present study therefore revisited the mathematics of the Weihs and Webb (1984) model to examine how deviation from optimal strategy affects prey evasion. We expanded this model and performed numerical simulations for comparison with experimental results. In this effort, we arrived at new interpretations of theory on prey evasion. In particular, we identified conditions where the escape direction is predicted to have little or no effect on the evasiveness of prey.

1.2.1 Optimal prey strategy

The Homicidal Chauffeur is the colorful title for a pursuit–evasion game that has been applied to a variety of systems, including predator–prey interactions (Isaacs, 1965). Pursuit–evasion games consider the trajectories of its players and thereby address the effects of directional decision–making to the outcome of an interaction. Weihs and Webb (1984) adopted the Homicidal Chauffeur to model the responses of a prey fish that encounters a predator fish. Here we offer a brief review of this model as a means to explain the basis for our expansion of the theory and our interpretations of prey strategy, though a more complete derivation is presented in the original study (Weihs and Webb, 1984).

The payoff is a quantity used in game models to define the beneficial or detrimental consequences of playing with a particular strategy (Webb, 2007). For the Homicidal Chauffeur, the payoff is often defined as the minimum distance between predator and prey. This quantity reflects the condition where the predator has the best opportunity to capture the prey. The optimal strategy for an evasive prey is therefore defined as the escape angle that yields the greatest minimum distance (Weihs and Webb, 1984).

Predicting the distance between predator and prey requires relatively few parameters under some simplifying assumptions. In the rapid events of a predatory strike, it is reasonable to approximate the predator's motion as a constant speed, U. If one neglects the acceleration period of the fast start, then the prey's motion may also be approximated with a constant speed, V, at an escape angle α, defined with respect to the heading of the predator (Fig. 1.2A). Under these conditions, the distance between predator and prey, D, may be calculated over time:

$$D^2 = ((X_0 - Ut) + Vt\cos\alpha)^2 + (Vt\sin\alpha)^2, \tag{1.1}$$

where X_0 is the starting position of the prey.

The minimum distance, the payoff in this game, may be calculated from the distance equation. The first step is to calculate the time, $t_{\min}$, at which the minimum distance occurs. This may be found from the root of the derivative of Eqn. 1.1 with respect to time, which yields the following equation:

$$t_{\min} = \frac{X_0}{V}\frac{K - \cos\alpha}{1 - 2K\cos\alpha + K^2}, \tag{1.2}$$

where K indicates the speed of the predator relative to the prey ($K = U/V$). This equation yields negative values of time where $K < 1$ and therefore only applies where $K > 1$. The minimum distance was consequently determined for $K > 1$ by solving for distance (Eqn. 1.1) at $t_{\min}$:

$$\overline{D}^2_{\min} = \frac{D^2_{\min}}{X_0^2} = \frac{\sin^2\alpha}{K^2 - 2K\cos\alpha + 1}, \tag{1.3}$$

where $\overline{D}_{\min}$ is the minimum distance normalized by the starting position of the prey.

Finally, the optimal strategy for the prey may be determined by finding the escape angle that yields the greatest minimum distance. This occurs where the derivative of Eqn. 1.3

with respect to α is equal to zero, which is explicitly described by the following equation:

$$0 = \frac{\partial \overline{D}^2_{\min}}{\partial \alpha} = \frac{2 \sin \alpha \cos \alpha (K^2 - 2K \cos \alpha + 1) - 2K \sin^3 \alpha}{(K^2 - 2K \cos \alpha + 1)^2}. \tag{1.4}$$

Among the solutions that satisfy this equation, Weihs and Webb proposed that the following indicates the optimal strategy when the predator is faster than the prey ($K > 1$):

$$\alpha_{\text{opt}} = \pm \arccos K^{-1}. \tag{1.5}$$

We added the $\pm$ symbol to this expression to indicate that prey are equally effective if escaping at an optimal angle toward the left ($\alpha > 0$), or right ($\alpha < 0$) of the predator's heading. For relatively fast prey ($K < 1$), Weihs and Webb suggested that the optimal solution consists of swimming directly away from the predator ($\alpha = 0$) (Weihs and Webb, 1984). Therefore, for any predator speed, this model offers predictions for how a prey can direct its escape to maximize its chances for survival by creating the greatest distance from a predator.

1.3 When optimal strategy matters

An optimum adopts a different meaning if it corresponds to a sharp global maximum, a local peak much smaller than the global maximum, or a shallow peak in performance. We considered the conditions exist that surround optimal strategy by calculating how the payoff in this pursuit model, the minimum distance (Weihs and Webb, 1984), varies with escape angle and the relative speed of the predator. As an alternative to analytical mathematics, we first formulated this performance landscape with a numerical approach that is simple enough to execute in a spreadsheet, but which we implemented in Matlab (v2014b, MathWorks, Natick, MA, USA). This was done by defining a series of time values

at a regular interval, which was used to calculate the positions of the predator ($X_{\text{pred}} = Ut$, $Y_{\text{pred}} = 0$) and prey ($X_{\text{prey}} = Vt\cos\alpha, Y_{\text{prey}} = Vt\sin\alpha$). The minimum value of the distance between them was determined in this way for variable escape angle and predator speed, over a range of K and α values (Fig. 1.2B). This yielded results that were coincident with the analytical equation for $\overline{D}_{\text{min}}$ formulated by Weihs and Webb (1984) for relatively fast predators ($K > 1$, Eqn. 1.3). However, the advantage of this numerical calculation was that it allowed us to examine variation in the minimum distance for slower predators (i.e. $K < 1$) as well. The resulting performance landscape (Fig. 1.2B) illustrates how the minimum distance varies over a broad range of values in the relative speed of the predator.

Our results suggest that the fast start is unlikely to be effective at any escape angle when a prey is approached by a very fast predator. For example, if a predator is an order of magnitude faster than its prey (i.e. $K = 10$), then the prey can do no better than displace its body by 10% of its initial distance (Fig. 1.2B). In addition, differences in escape angle have little effect on the minimum distance. Specifically, an escape that is 24.5 ° larger or smaller than the optimum yields a minimum distance that is less than the value at the optimum by 0.1 (i.e. 1% of the starting position of the prey). These metrics become increasingly unfavorable for the prey when approached by an even faster predator (Fig. 1.2B). At these speeds, inaccuracy in the feeding strike is likely a more decisive factor to prey survival than anything the prey may do in response.

A different picture emerges when one considers prey that move more quickly than their predators (i.e. $K < 1$). This condition occurs when predators brake or glide slowly on their approach toward a prey (Higham, 2007; Higham et al., 2005) while the prey initiates a rapid escape. For a variety of escape angles, the fast start of these prey cause the predator to reach no closer than the starting distance (i.e. $\overline{D}_{\text{min}} = 1$, Fig. 1.2B). In order to define the bounds of this domain, it is useful to consider the first derivative of the distance function

with respect to time (see Supplemental Materials for details):

$$\frac{\partial D^2}{\partial t} = 2(t(U^2 + V^2) - UX_0 + V(X_0 - 2tU)\cos\alpha). \tag{1.6}$$

An optimal escape ($\overline{D}_{\min} = 1$) can be achieved if the distance function increases for all time (i.e. $\frac{\partial D^2}{\partial t} \geq 0$). This holds true for $\alpha = 0$, which Weihs and Webb proposed as the optimal direction (Weihs and Webb, 1984). However, it also holds true that distance increases for another solution to Eqn. 1.4 ($\alpha = \pm \arccos K$) and all values in between (see Supplemental Materials for details). Therefore, the following defines the domain of optimal directions when the prey is faster than the predator ($K < 1$):

$$\overline{D}_{\min} = 1 \quad \text{if} \quad |\alpha| \leq \arccos(K). \tag{1.7}$$

This analysis suggests that if the escape response of a prey is capable of exceeding the approach speed of the predator, then a wide range of angles yield equally successful escapes for the prey and thereby define a performance plateau.

The domain where the optimal strategy matters the most resides between where the prey and predator are equivalent in speed and where the predator is an order of magnitude faster ($1 < K < 10$). In this domain, prey are capable of attaining appreciable minimum distance values and there is a penalty in minimum distance for deviating from the optimal angle (Fig. 1.2B). Therefore, a prey fish has a strong incentive to conform to the optimal prediction when encountering a predator that can move slightly faster than itself.

1.4 Comparing models with measurements

We were interested in examining whether optimal strategy matters under experimental conditions. This was addressed with recent measurements on larval zebrafish, which were preyed upon by adults of the same species (Stewart et al., 2013). This work included experiments that used a robot to simulate the approach of a predator toward prey in the dark, with recordings of the position at which the prey responded with a fast start and the direction of that response (Stewart et al., 2014). This evasive action was stimulated by the lateral line system of the prey, which detected the water flow generated by the approaching predator.

As detailed above, the predictions of the model depend on the speed of the predator relative to the prey. The approach speed of the robot, and consequently K, was varied to span the range of values observed for a live predator (Stewart et al., 2013). Our calculations of K used a prey speed ($U = 22\,\mathrm{cms}^{-1}$) from the literature that approximates the maximum value attained during a fast start for larvae of this species (Budick and O'Malley, 2000; Müller and van Leeuwen, 2004). As a consequence of the relatively slow approach made by these suction–feeding predators, the prey had the potential to move faster at all approach speeds, which yielded K–values that were uniformly less than unity (Fig. 1.3A).

One discrepancy between the model and our experiments was that the majority of prey fish did not exhibit an initial position that was aligned with the heading of the predator robot. This condition has biological relevance because it corresponds to a situation where a predator fails to approach a prey with perfect accuracy. We therefore modified the Weihs and Webb model by adding a lateral component to the initial position of the prey in our distance function. Following the same procedure (Eqns. 1.2–1.3), we arrived at a minimum distance function (see A for details). This function was simplified by the use of polar

coordinates, as in the following equation:

$$\overline{D}_{\min}^2 = \frac{D_{\min}^2}{R_0^2} = \frac{(\sin(\alpha - \theta_0) + K \sin\theta_0)^2}{K^2 - 2K\cos\alpha + 1} \tag{1.8}$$

where R_0 and θ_0 are the initial radial and angular positions of the prey relative to the mouth of the predator (Fig. 1.2A). Numerical solutions to this equation showed a broad range of angular positions and escape angles that defined a performance plateau where $D_{\min} = 1$ (Fig. 1.3B). We found the margins of this plateau using a similar procedure as outlined above (Eqn. 1.4). Specifically, we solved for the conditions where the derivative of the minimum distance with respect to α was equal to zero:

$$0 = \frac{\partial \overline{D}_{\min}^2}{\partial \alpha} = \frac{2(K\cos\alpha - 1)(K\cos\theta_0 - \cos(\alpha - \theta_0))(K\sin\theta_0 + \sin(\alpha - \theta_0))}{(K^2 - 2K\cos\alpha + 1)^2}, \tag{1.9}$$

We found the solutions that satisfy this equation by setting the terms in the numerator equal to zero. The solution for $K > 1$ and $\theta_0 < \arccos(K^{-1})$ was similar to Eqn. 1.5, though the initial angular position determines the sign of the optimal angle:

$$\alpha_{\text{opt}} = \frac{\theta_0}{|\theta_0|}\arccos(K^{-1}). \tag{1.10}$$

This solution indicates that the same optimal direction exists when the predator is faster than the prey, irrespective of the prey's initial position up to an initial angular position of $90\,^\circ$. As detailed above, we found that the escape angle is equally effective (i.e. $\overline{D}_{\min} = 1$) when the prey is aligned with the predator for a broad range of values (Eqn. 1.7). This result holds true when prey are positioned lateral to the predator, but this performance plateau depends on the initial angular position of the prey. We found that the following equation defines the bounds of this plateau among the solutions that satisfy Eqn. 1.8 for $K < 1$:

$$\overline{D}_{\min} = 1 \quad \text{if} \quad |\alpha - \theta_0| \leq \arccos(K\cos\theta_0), \tag{1.11}$$

This demonstrates that the performance plateau reduces in area with increasing predator speed (Fig. 1.3B). Therefore, fewer combinations of starting positions and escape angles yield equivalent escape performance for faster predators.

Using this formulation of the pursuit–evasion model, we evaluated how the measured responses of prey compared to the model predictions (Fig. 1.3C). This revealed that the vast majority of larvae operated within the performance plateau and therefore were predicted to yield maximal performance ($\overline{D}_{\min} = 1$). This was true even at the fastest predator approach speed ($K = 0.90$), where the performance plateau encompasses a smaller area of the performance landscape. Therefore, the large variation in observed escape direction incurs no penalty in the evasive performance of most larvae.

1.5 Predator strategy

Although the present pursuit–evasion models were formulated with a focus on prey fish, they provide the opportunity to consider the strategy of fish predators. The payoff considered by these models is normalized by the initial response distance of the prey (Figs. 1.2–1.3). Because the absolute distance traversed is therefore predicted to be proportional to the initial response distance, the predator may first do well to minimize this distance. This may be achieved by moving with a slower approach to reduce the stimulus intensity for the visual (Dill, 1974) and lateral line (Stewart et al., 2014) systems that could startle the prey. This is one benefit to the braking behavior that suction–feeding predators exhibit before a strike (Higham, 2007; Higham et al., 2005). Another advantage to a slow approach is the potential for greater accuracy in the timing and direction of a suction–feeding strike, which is restricted to a brief duration over a relatively small region around a predator's mouth (Wainwright et al., 2001).

Our results also indicate some of the strategic advantages for fast predators. Moving faster than the escaping prey greatly diminishes the escape angles that are beneficial for evasion (Fig. 1.2B). As we discussed above (in Section 1.2.1 "Optimal prey strategy"), the fast start can become ineffective at offering any benefit to predator evasion when the predator is substantially faster and headed directly at the prey. However, such a high–speed approach may present a challenge for a predator to coordinate the timing of the strike (Higham, 2007; Higham et al., 2005).

We conducted a series of simulations that examine the effect of an inaccurate strike by a fast predator. As in our comparison with experimental results (Fig. 1.3), we calculated the minimum distance for a range of values in escape angle and initial position, but this time considered predators that were faster than prey ($K > 1$). We interpreted deviation from a zero angular position as a measure of inaccuracy in the strike of the predator with the assumption that fish lack the interception targeting used by bats (Ghose et al., 2006) and birds (Kane and Zamani, 2014). This measure of inaccuracy neglects the increasing challenge of correct timing in the opening of the jaws at increasing approach speeds (Kane and Higham, 2014, 2011), but does address errors in the direction of the approach.

The results of these simulations illustrate the relative contribution of escape angle and strike accuracy on evasion for different approach speeds. For a predator that is twice as fast as the prey ($K = 2$), the minimum distance varied substantially with both escape direction and strike accuracy (Fig. 1.4A). For example, the optimal escape angle ($\alpha_{\text{opt}} = 60.0\,^\circ$) generated a minimum distance ($\overline{D}_{\text{min}} = 0.71$) that was more than two-orders of magnitude better than what was achieved with the least effective escape direction ($\overline{D}_{\text{min}} = 0.002$) when the prey is positioned $15\,^\circ$ from the predator's heading. This advantage in minimum distance was not greatly reduced ($\overline{D}_{\text{min}} = 0.50$ at $\alpha_{\text{opt}} = 60\,^\circ$) if the predator successfully aligned its strike ($\theta_0 = 0\,^\circ$). However, the escape angle played a reduced role in aiding predator evasion at faster approach speeds. For example, when the predator was 10-times

faster (Fig. 1.4C) and inaccurate ($\theta_0 = 15\,^\circ$), then the optimal escape angle ($\alpha_{\text{opt}} = 84.3\,^\circ$) was only slightly more than twice the value ($\overline{D}_{\text{min}} = 0.35$) for the least effective angle ($\overline{D}_{\text{min}} = 0.16$). Furthermore, the optimal minimum distance ($\overline{D}_{\text{min}} = 0.10$) was relatively ineffective for an accurate strike ($\theta_0 = 00\,^\circ$). Therefore, the accuracy of a predators' strike becomes an increasingly dominant factor in determining prey survival with predators that are many times faster than the prey.

1.6 Conclusions

The results of our modeling demonstrates theoretical conditions where the optimal strategy of prey matters little to the outcome of a predatory strike. These conditions depend on the relative speed of the predator and prey, which underscores the coupled nature of pursuit strategy. When a predator approaches relatively slowly, prey have the opportunity to escape in a variety of directions (Figs. 1.2B, 1.3B–C). When they strike quickly, the accuracy of the predator's heading becomes a major determinant in the outcome (Fig. 1.4). These interpretations have the potential to inform our reading of previous studies. However, the behavior of predator and prey fish are rarely studied simultaneously and the relative speed of predator and prey are seldom reported. Therefore, the present modeling may be most useful in offering a framework for future investigations.

It may appear counter-intuitive that any predator would move more slowly than its prey. Predatory fishes are commonly between 2- and 20-fold greater in length than their prey (Fuiman, 1994) and are generally capable of swimming many times their body length per second by rapid undulation (Bainbridge, 1958). However, fishes also exhibit a large scope of swimming speeds and may move slowly by the coordinated braking action of their many fins (Videler, 1981; McHenry and Lauder, 2005). Many suction-feeding predators take advantage of this hydrodynamic plasticity to slow swimming on the approach of a feeding

strike. This braking results in swimming that is in the lower range of potential speeds, at rates below a single body length per second (Higham et al., 2005; Higham, 2007). In contrast, a startled prey may act to maximize its proximity from a predator with its fastest swimming possible. Even a larval fish may attain speeds in excess of $50\,\mathrm{BLs}^{-1}$ during a fast start (Müller and van Leeuwen, 2004). Therefore, prey may compensate for their smaller size if the predator brakes for suction feeding to yield a condition where$K < 1$ (Fig. 1.3).

When a prey swims faster than a predator escape may be successful in a variety of directions (Eqn. 1.11). Any escape in this domain prohibits the predator from getting any closer than the distance at which the prey initiates its escape (Fig. 1.3). This strategic benefit is compatible with our thinking about the motor control of the escape response. Zebrafish larvae respond to a robotic predator with directionality that is no more specific than moving away from the side of the body exposed to a faster flow stimulus (Stewart et al., 2014). Such crude decision-making may be achieved through relatively few synapses that serve to create motion with brief latency (Liu and Fetcho, 1999). The present results suggest that there is little strategic disadvantage to this motor control. A shorter latency allows the prey to respond at greater distance and the direction of most responses is equally effective, even for the fastest predator (Fig. 1.3C).

It could be suggested that a failure of prey to conform to a single escape direction indicates deviation from optimal strategy. The benefit to a population of prey responding this way is that they become unpredictable to predators (Humphries and Driver, 1970). However, our view is that a performance plateau, and not an optimum, permits maximal evasiveness for a large range of escape directions (Fig. 1.3B–C). Therefore, no trade-off exists in this domain between predictability and evasiveness.

Different strategic dynamics come into play when the predator is faster than the prey. At intermediate speeds ($1 < K < 10$), deviation from optimal strategy has the potential for

large adverse consequences (Fig. 1.2B, 1.4A–B) and it is therefore in this domain that optimal strategy is most likely to be meaningful for the prey. To move in the optimal direction, the prey must detect the heading and speed of the predator, which is likely to be achieved by the visual or lateral line systems (Stewart et al., 2013; Dill, 1974; Paglianti and Domenici, 2006; Higgs and Fuiman, 1996). It is additionally necessary that the motor system be capable of rapidly propelling the fish in the optimal direction. As noted by Domenici, constraints on the sensory and motor systems can prohibit a prey from conforming to an optimum (Domenici and Blagburn, 2011a).

Sensory-motor constraints may play a role in guppies (*Poecilia reticulata*) that are preyed upon by pike cichlids (*Crenicichla alta*) (Walker et al., 2005). These predators are approximately twice as fast as the prey and the prey escape in a variety of directions. The survivorship was also higher in prey that escaped directly away from predators ($\alpha \sim 180\,^\circ$) than those which responded in the optimal direction that our model would predict ($\alpha_{\text{opt}} = 60\,^\circ$). It is alternatively possible that the pike may accelerate to a degree that substantially violates the assumptions of our model.

Our model predicts that the accuracy of a predator's strike becomes a dominant factor in the outcome of an interaction for predators that approach at high speed ($K > 10$). In this domain, differences in minimum distance amount to minor performance differences cross a broad range of escape angles (Fig. 1.2B). It remains possible that these differences in distance are more meaningful to the hydrodynamics of prey evasion when the predator is attempting a rapid strike. Resolving this issue would require an explicit consideration of hydrodynamics (as in Holzman et al., 2011).

1.7 Figures

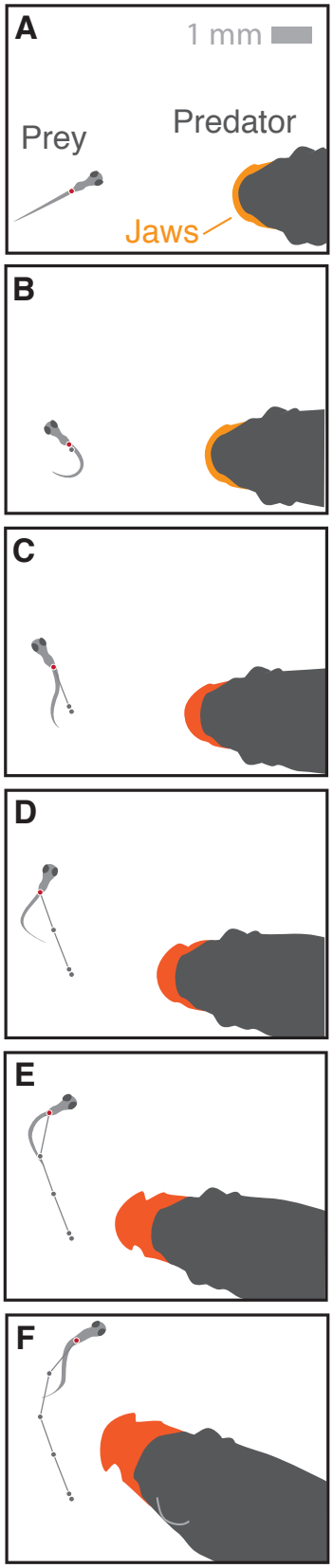

Figure 1.1: A predator-prey interaction in zebrafish. Silhouettes of zebrafish from a dorsal perspective have been traced from video stills (5 ms interval) as an adult attempts to capture a larva with a suction feeding strike. (**A**–**B**) On the predator's approach, the prey initiates a 'fast-start' escape response to accelerate away from the predator. The strike has yet to begin, as shown by the lack of protrusion by the jaws of the predator (orange). (**C**–**D**) The predator initiates a strike, which is visible from jaw protrusion (red). (**E**–**F**) With its jaws fully extended, the predator fails to capture the prey which proceeds to move away from the predator with rapid undulatory swimming. Recording from Stewart et al. (2014).

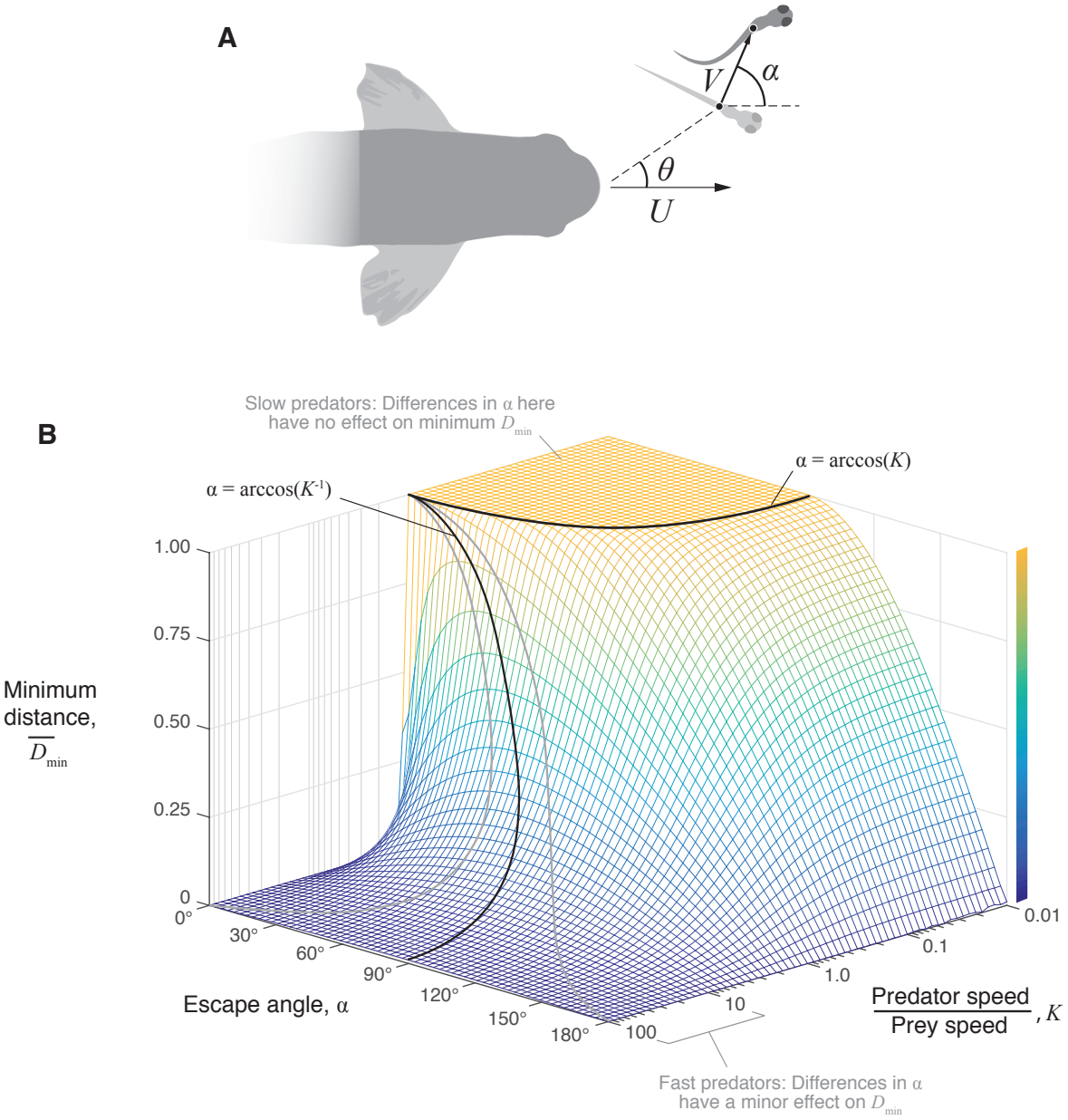

Figure 1.2: A pursuit–evasion model for predator–prey interactions in fish. (**A**) Pursuit–evasion models consider the motion of a predator (viewed from dorsal perspective) with speed U and a prey with speed V and escape angle α. Some versions of this model consider prey positioned lateral to the predator's approach ($\theta_0 > 0$). (**B**) Numerical simulations were run at varying escape angle and predator approach speed (with $\theta_0 = 0$) to examine variation in the minimum distance. At $K > 1$, the optimal angle (black curve) was predicted analytically (Eqn. refK¿1 by Weihs and Webb (1984). Deviation from the optimum by $0.1\overline{D}_{\text{min}}$ (gray curves) is shown to increase at greater values of K. The performance plateau where $D_{\text{min}} = 1$ is predicted by Eqn.1.7.

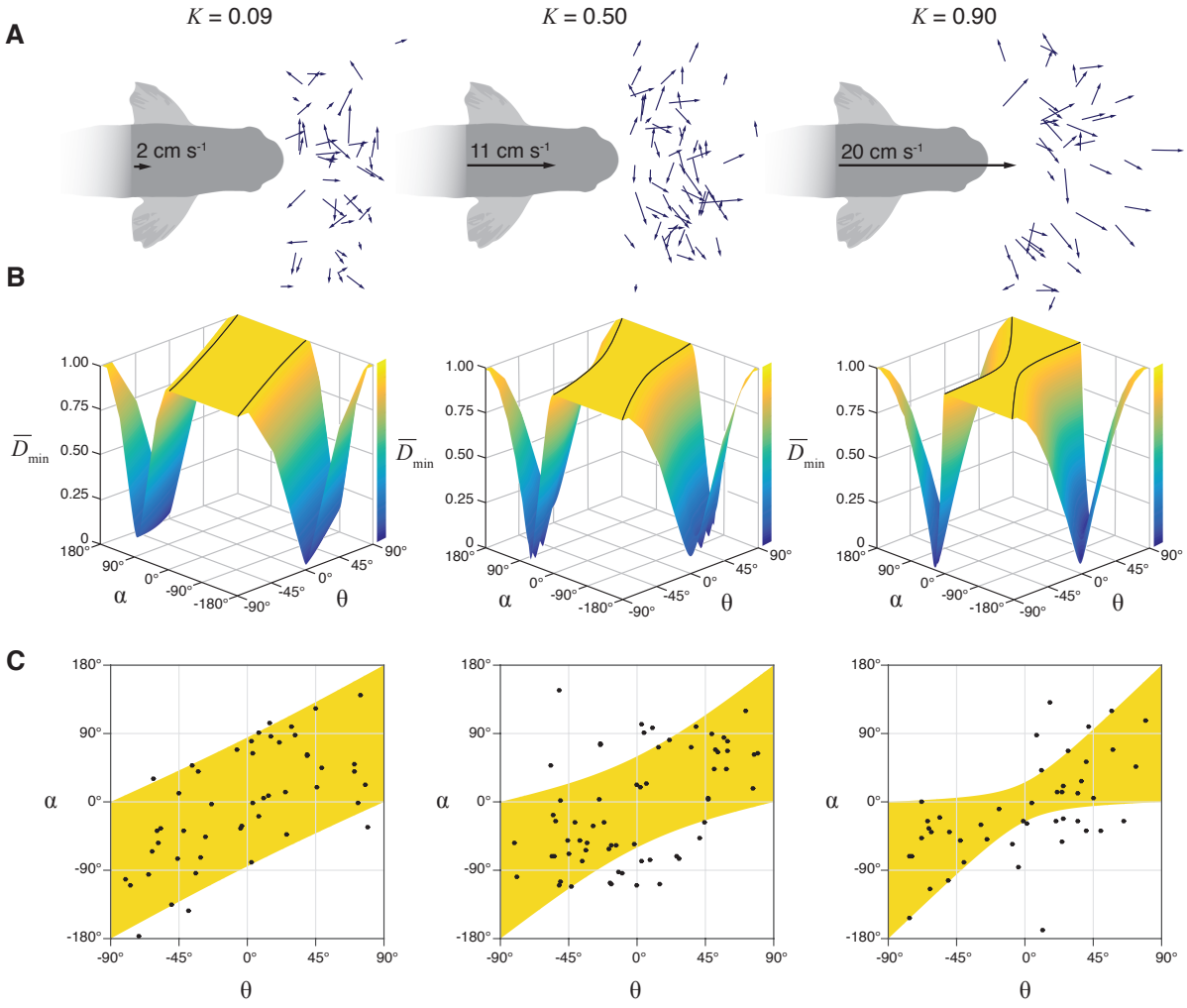

Figure 1.3: Model predictions and measurements of the fast start. The pursuit–evasion model was compared with experiments that recorded the responses of larval zebrafish that were approached by a robotic predator at three speeds (2, 11 and 20 cm s^{-1}) (Stewart et al., 2014). The results of experiments and modeling are arranged in column that correspond to each of these speeds. (**A**) The fast–start responses are illustrated by the center–of–body displacement for the two stages of the behavior (blue arrow). (**B**) Numerical results of the simulated interactions show how the minimum distance ($\overline{D}_{\min}$) varies with the escape angle(α) and initial position (θ_0). The plateau region (defined by Eqn. 1.7) shows an area where $\overline{D}_{\min} = 1$. (**C**)This area (in yellow) is plotted with measurements of the initial position and escape angle of the measured responses shown in **A**.

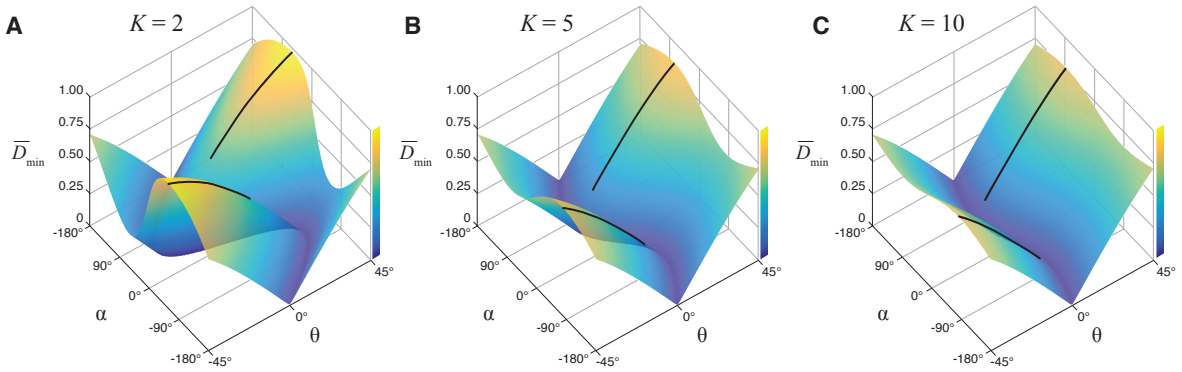

Figure 1.4: Evasive performance when the predator is faster than the prey. Numerical simulations calculated the minimum distance for variable initial position (θ_0) and escape angle (α) of the prey for predators that are faster than the prey by a factor of two (**A**), five (**B**), and ten (**C**).

Chapter 2

Zebrafish locomotion and trajectory control during active pursuit

2.1 Abstract

A fish predator's survival depends on its ability to chase down prey. Their pursuit strategy often depends on the ability to sense the location of prey and maneuver toward it. Unlike flying predators, many fish predators move in discrete, burst-and-coast bouts of activity. To understand the biomechanics of active pursuit with intermittent locomotion, we conducted predation experiments in zebrafish. Zebrafish accelerated and turned toward their prey during each burst phase, which was identified by a single tail beat. The change in heading during a tail beat could be predicted by the bearing angle preceding the burst phase and was correlated with the lateral excursion of the tail fin. This intermittent pursuit strategy is a form of pure pursuit in which the predator aligns its heading with the position of the prey. To investigate the mechanisms of directional control during intermittent pure pursuit,

we are developing a biomechanical model that simulates active pursuit. This work provides insight into the biomechanics of active pursuit of a broad diversity of aquatic predators.

2.2 Background

Successful predation is critical for the survival of animals and depends on their ability to sense and chase down prey. The strategies implemented by predators to track and capture prey vary widely among animals. Biologists have successfully applied mathematical models developed for missile guidance (Yuan, 1948; Shneydor, 1998) to determine the pursuit strategies of flying predators, such as dragonflies (Olberg et al., 2007; Mischiati et al., 2015), bats (Ghose et al., 2006), and raptors (Kane and Zamani, 2014; Kane et al., 2015; Brighton et al., 2017). These models generally assume continuous motion, but many predators move through their environment in discrete bouts of activity, such as the burst-and-coast swimming of zebrafish. The aim of this study was to determine the pursuit strategy of zebrafish, an intermittent swimmer, during active pursuit of evasive prey.

Kinematic measurements of pursuit trajectories can be compared with predictions of mathematical models to determine a predator's pursuit strategy. Two pursuit strategies commonly observed in nature are known as pure pursuit and interception (Nahin, 2007). The bearing angle (ϕ), defined as the angular position of the prey relative to the predator's heading (Fig. 2.1B), is useful for distinguishing between these two pursuit strategies. A predator implementing pure pursuit aligns its heading with the instantaneous position of the prey, while interception requires that the predator move toward the anticipated point of collision. If a predator is implementing a pure pursuit strategy, then we expect the bearing angle to be maintained at or driven to zero ($\phi \to 0$) during its approach toward the prey (Fig. 2.1C, $\phi = 0$). Alternatively, an interception strategy requires that the predator adopt a constant, optimal bearing angle (ϕ_{opt}), which is determined by the initial geometry of the interaction (Fig. 2.1C, $\phi \neq 0$). Aerial predators have been shown to implement a type of interception strategy known as proportional navigation (e.g., Brighton et al., 2017; Mills et al., 2018). These strategies require the predator to sense and maneuver toward its prey.

Vision is the dominant sensory modality in this behavior for fish as it allows for the greatest detection distance (Dill, 1974) in bright conditions and thus serves as input to the neural controller. The input sensory signals are used to determine the necessary motor commands for trajectory control (Tytell et al., 2011; Roth et al., 2014). Appropriate maneuvering is required to execute the pursuit strategy against evasive prey.

It is unclear whether predatory fish employ a common pursuit strategy as has been found for aerial predators. Recent work from our lab has shown that bluefish pursue evasive prey with a strategy known as deviated pursuit (McHenry et al., 2019), an intermediate strategy between pure pursuit and interception. Bluefish engage in fast, continuous pursuit that share many qualities with the pursuit behavior of aerial predators. Due to the intermittent swimming style of zebrafish, we do not expect them to employ such a strategy. In the present study, we use kinematic measurements of zebrafish during active chase sequences to determine its pursuit strategy. Biomechanical modeling allowed us to test the role of the caudal fin in controlling the predator's trajectory toward prey. This work provides insight into the biomechanics of active pursuit of a broad diversity of aquatic predators.

2.3 Materials and methods

2.3.1 Experiments

To investigate the targeting strategy of zebrafish, we built an experimental setup to film predator–prey interactions (Fig. 2.1A). We used a high-speed video camera (FASTCAM Mini AX100, Photron, San Diego, CA, USA) with high spatial resolution (1024×1024 pixels) configured with a macro lens (Micro-Nikkor 105 mm $f/2.8$, Nikon Inc., Melville, NY, USA). To visualize the predator and prey, three infrared (IR, 940 nm) LED panels were placed below a translucent white acrylic diffuser, which was placed below the predation arena. This

generated a high-contrast image of the fish with transmitted illumination. A white LED panel placed above the arena provided reflected illumination. The camera was placed in front of the arena and directed at a mirror oriented at 45 ° from the horizontal to visualize the fish from a dorsal perspective.

Predation experiments were performed with $n_{\text{pred}} = 38$ (1.49 cm $\pm$ 0.43 cm, standard length) predator and $n_{\text{prey}} = 31$ (5$-$13 dpf) prey zebrafish (*Danio rerio*, Hamilton 1822) maintained in a recirculating freshwater system at 27 °C on a 14 L:10 D cycle. For each predator-prey pair, fish were transferred to the predation arena and separated by an acrylic divider. We waited at least 10 min. prior removing the divider and filming. We stopped recording and saved the sequence to disk when the predator completed an active chase, which was defined as the moment when the predator either captured the prey or ceased moving toward the prey. We filmed $n_1 = 31$ active chase sequences of varying duration and $n_2 = 22$ sequences of the predator fish swimming without the prey present. All experiments were conducted in accordance with the University of California, Irvine's Institutional Animal Care and Use Committee (Protocol #AUP-17-012).

2.3.2 Image processing and data analysis

Our recordings of the fish were analyzed to automate tracking of the prey's position and the predator's body midline. This procedure, and all data analyses, were performed by programming within MATLAB (v.2014b, MathWorks, Natick, MA, USA). Our program employed the image processing task generally known as blob analysis which requires the conversion of grayscale images into binary images by defining an intensity value that partitions dark and light pixels, designated as background and foreground, respectively. This image segmentation technique, known as thresholding, generates 'blobs' of connected pixels from which features (e.g. centroid and area) may be calculated.

The high spatial resolution of our experimental setup combined with the size differential of the predator and prey allowed for automated blob analysis for both fish and midline tracking of the predator (Fig. 2.2A). We used an input reference image for background subtraction and applied a local thresholding technique ('adaptthresh' function in MATLAB) that is robust to nonuniform illumination. The resulting binary image (Fig. 2.2A, ii) described the shape of the fish's body, which we refined with morphological operations to fill holes and connect any gaps with neighboring blobs. The prey fish blob was manually selected in the first video frame and subsequently identified by its area and proximity to the previous frame's blob. For each frame, we measured the blob's area and identified its center-of-area (red dot in Fig. 2.2A, ii). The predator blob was identified by a similar procedure and its midline was extracted. The midline was identified by distance mapping, which encodes a value for each pixel of the blob according to its distance to the nearest background pixel (Fig. 2.2A, iii). We applied distance mapping along the rows and columns of the binary image and the resulting maps were concatenated to produce the set of pixels that define the predator's midline. For kinematic analysis, the raw midline coordinates for each video frame were smoothed with the 'loess' method, a locally weighted polynomial regression (Fig. 2.2A, iv). We extracted several positions along the predator's midline to compute its heading, center-of-mass velocity, and angular position of the caudal peduncle and fin. The final result was a kinematic dataset for the prey's body and the predator's midline that was obtained automatically.

For each active chase sequence, we identified every tail beat and coast phase from the predator's time series data (Fig. 2.2B). A discrete tail beat was identified by the interval of nonzero values of angular velocity, $\dot{\theta}(t)$, which signify that the heading, $\theta(t)$, is changing. The coast phases were identified as the intervals where heading was relatively constant or $\dot{\theta} = 0$. To assess the predator's pursuit strategy, we measured the angular position of the prey relative to the predator's heading (Fig. 2.1B). This angle (ϕ) is known as

the bearing angle and its value through time may be used to interpret the predator's pursuit strategy. To determine which pursuit strategy (pure pursuit or interception) best described the predator's behavior, we used a linear regression (Model 2 regression) between the expected and measured bearing angle. Since we did not observe an effect of distance between predator and prey, we treated each turn during an active chase as independent events.

2.3.3 Mathematical modeling of predator locomotion

The aim in modeling the predator's locomotion was to gain an understanding of how the swimming hydrodynamics affect the pursuit trajectory. Mathematical models of swimming range from simple, one-dimensional kinematic models to complex, three-dimensional models that require computational fluid dynamics (Borazjani and Sotiropoulos, 2008; Miller et al., 2012) simulation. Due to a growing interest from the robotics community in biomimetic swimmers (e.g., Morgansen et al., 2007; Suebsaiprom and Lin, 2015; Wang et al., 2015; Scaradozzi et al., 2017; Gravish and Lauder, 2018), we opted for a dynamic model that would be amenable for robot optimization and control rather than a complete description of the fluid-body interaction. We therefore modeled the fish as a rigid body attached to a tail, which is actuated at the base. The tail is composed of two segments connected in series through a torsion spring and viscous damper. In the following sections we describe the rigid-body dynamics for the fish body and the hydrodynamic force model for the tail.

2.3.3.1 Rigid-body dynamics

The equations of motion for the swimming predator in a fixed $X - Y$ plane are given by

$$\mathbf{F} = m_b \mathbf{a}, \tag{2.1}$$

$$\mathbf{M} = I_b \mathbf{\Omega}, \tag{2.2}$$

where $\mathbf{F}$, $\mathbf{M}$ are the external forces and moments exerted on the body about the center of mass (COM), m_b and I_b are the mass and moment of inertia of the body, and $\mathbf{a}$ and $\mathbf{\Omega}$ are the translational and angular acceleration of the body in the inertial reference frame. Since we assume planar motion, we have $\mathbf{a} = (\ddot{x}, \ddot{y})$ and $\mathbf{\Omega} = \ddot{\theta}$, where $\mathbf{v} = (\dot{x}, \dot{y})$ and $\dot{\theta}$ are the COM translational and rotational velocity of the body, respectively. These quantities represent the three degrees of freedom for the planar rigid body.

We further assume that the fish body and tail are neutrally buoyant. Therefore, the external forces and moments are due only to hydrodynamic interactions between the fish body and tail with the fluid. These include the hydrodynamic force and moment generated by the motion of the tail (described in the following subsection) as well as drag force $\mathbf{F}_D$ and drag moment M_D on the body.

The drag on the body is given by

$$\mathbf{F}_D = -\left(\frac{1}{2}\rho C_d S \|\mathbf{v}\|\right)\mathbf{v}, \tag{2.3}$$

where ρ is the density of the fluid ($1,000\,\mathrm{kg/m^3}$), C_d is a dimensionless drag coefficient, S is the wetted surface area of the fish. The drag moment is given by

$$M_D = -C_M \mu L^3 \dot{\theta}, \tag{2.4}$$

where C_M is a dimensionless drag moment coefficient, L is a characteristic length, and μ is the dynamic viscosity of the fluid.

2.3.3.2 Hydrodynamics of tail model

In this section, we describe the hydrodynamic forces generated by the motion of the tail. The tail is attached to the rigid body through a passive joint and is composed of two rigid segments, which represent the peduncle and caudal fin of the fish. The tail segments are linked through a joint modeled as a torsion spring and viscous damper. The rotational joints connecting the three segments have joint angles ψ_1 and ψ_2. For simplicity, we assume that there is no hydrodynamic interaction between the two tail segments. Therefore, the hydrodynamic forces are generated solely by the motion of the posterior caudal fin section.

Let l_b be the distance between the body COM and the peduncle, l_p the length of the peduncle, and l_f the length of the fin with surface area S_{fin}. Note that ψ_1 is measured relative to the longitudinal body axis and ψ_2 is measured relative to the peduncle orientation. Let $\eta = \theta + \psi_1 + \psi_2$, which is the angle of the fin relative to the inertial $x-$axis. Then the velocity at the fin's quarter chord point is given by

$$\mathbf{v}_{qc} = \begin{pmatrix} \dot{x} + l_b \sin\theta(\dot{\theta}) + l_p \sin(\theta+\psi_1)(\dot{\theta}+\dot{\psi_1}) + \dfrac{l_f}{4}\sin\eta(\dot{\eta}) \\ \\ \dot{y} - l_b \cos\theta(\dot{\theta}) - l_p \cos(\theta+\psi_1)(\dot{\theta}+\dot{\psi_1}) - \dfrac{l_f}{4}\cos\eta(\dot{\eta}) \end{pmatrix} \tag{2.5}$$

We calculated the Reynolds number (Re) for the caudal fin in our experiments and found that $Re_{fin} \approx 150$. In this fluid regime, both viscous and inertial forces play a significant role in the fluid dynamics. As a consequence, we used a quasi-steady lift and drag model (Dickinson et al., 1999; Morgansen et al., 2001; Sane and Dickinson, 2002) of the forces on

the fin. These forces are defined as

$$\mathbf{L}_{fin} = \frac{1}{2}\rho C_{L(\alpha)} S_{fin} \|\mathbf{v}_{qc}\| \mathbf{v}_{qc} \tag{2.6}$$

$$\mathbf{D}_{fin} = \frac{1}{2}\rho C_{D(\alpha)} S_{fin} \|\mathbf{v}_{qc}\| \mathbf{v}_{qc}, \tag{2.7}$$

where $C_{L(\alpha)}$ and $C_{D(\alpha)}$ are the lift and drag coefficients, respectively. For a dynamically oscillating fin (or airfoil), the lift and drag forces are dependent on the angle between the local flow velocity and the orientation of the fin or angle of attack, α. This dependence is captured in our model by $C_{L(\alpha)}$ and $C_{D(\alpha)}$, which are based on experimental results on model insect wings operating at a similar Re (Dickinson and Götz, 1993; Dickinson et al., 1999; Sane and Dickinson, 2002).

2.3.3.3 Longitudinal and lateral body forces

By definition, drag is oriented in the negative direction relative to $\mathbf{v}_{qc}$ and lift is perpendicular to drag. The vector sum of $\mathbf{L}_{fin}$ and $\mathbf{D}_{fin}$ yields the resultant force $\mathbf{F}_{fin} = (F_x, F_y)$. Since these components are oriented along the inertial x and y directions, we premultiply $\mathbf{F}_{fin}$ by a rotation matrix R to get the longitudinal, $F_\parallel$, and lateral, $F_\perp$, components relative to the orientation of the body. That is,

$$\begin{pmatrix} F_\parallel \\ F_\perp \end{pmatrix} = \begin{pmatrix} \cos(\theta) & \sin(\theta) \\ -\sin(\theta) & \cos(\theta) \end{pmatrix} \begin{pmatrix} F_x \\ F_y \end{pmatrix} \tag{2.8}$$

2.3.3.4 Dynamic model equations

With the forces defined, we can now apply Eqns. (2.1)–(2.2) to obtain a system of ordinary differential equations (ODEs) that describe the motion of (x, y, θ).

Substituting $\mathbf{v} = v_x\mathbf{e}_x + v_y\mathbf{e}_y$ into Eqn. (2.3) yields

$$\mathbf{F}_D = -\left(\frac{1}{2}\rho C_d S\|\mathbf{v}\|\right)(v_x\mathbf{e}_x + v_y\mathbf{e}_y) = -\left(\frac{1}{2}\rho C_d S\|\mathbf{v}\|\right)v_x\mathbf{e}_x - \left(\frac{1}{2}\rho C_d S\|\mathbf{v}\|\right)v_y\mathbf{e}_y,$$

where $v_x = \dot{x}$, $v_y = \dot{y}$, and $\|\mathbf{v}\| = \sqrt{\dot{x}^2 + \dot{y}^2}$. The x and y components of the drag force are then

$$F_{D_x} = -\left(\frac{1}{2}\rho C_d S\|\mathbf{v}\|\right)\dot{x}, \tag{2.9}$$

and

$$F_{D_y} = -\left(\frac{1}{2}\rho C_d S\|\mathbf{v}\|\right)\dot{y} \tag{2.10}$$

Substituting the above into Eqn. (2.1) along the x and y directions and carrying out the multiplication in Eqn. (2.8), we obtain

$$m\ddot{x} = F_\parallel\cos\theta - F_\perp\sin\theta - \frac{1}{2}\rho C_d S\|\mathbf{v}\|\dot{x} \tag{2.11}$$

$$m\ddot{y} = F_\parallel\sin\theta + F_\perp\cos\theta - \frac{1}{2}\rho C_d S\|\mathbf{v}\|\dot{y} \tag{2.12}$$

Note that if $F_\parallel$ is the only component of thrust acting on the body, the motion is pure translation with direction θ. In order to change the heading, we must have a nonzero turning moment about the body COM. The turning moment, $\mathbf{M}$, is composed of the moment due to the hydrodynamic force generated by the tail, M_{fin}, and the drag moment, M_D. M_{fin} is found by taking the z-component of the following cross product

$$M_{fin} = (x_{qc}, y_{qc}, 0) \times (F_x, F_y, 0),$$

where $(x_{qc}, y_{qc}, 0)$ is the position of the fin's quarter chord point relative to the body COM. Substituting M_{fin} and M_D into Eqn. (2.2) we obtain the following

$$I_b\ddot{\theta} = x_{qc}F_y - y_{qc}F_x - C_M\mu L^3\dot{\theta}, \tag{2.13}$$

The system of ODEs is defined by Eqns. (2.11)–(2.13).

2.3.3.5 A note on second–order differential equations in MATLAB

The system equations describing the dynamics all contain the second derivative of the state variable. These are known as second–order differential equations. To solve this type of differential equation numerically, we must write each second–order equation as a system of two first–order equations. This is accomplished through a simple, but clever, substitution.

Let $\ddot{y} = f(y, \dot{y}, t)$ be any second–order differential equation. Set $y_1 = y$ and $y_2 = \dot{y}$. Then,

$$\dot{Y} = \begin{pmatrix} \dot{y_1} \\ \dot{y_2} \end{pmatrix} = \begin{pmatrix} y_2 \\ f(y_1, y_2, t) \end{pmatrix} \tag{2.14}$$

In this form, numerical solvers such as MATLAB 's ode45 can be utilized to solve the second-order ODE.

2.4 Results and discussion

We measured swimming kinematics of active pursuit in zebrafish. Predatory zebrafish swam in a burst-and-coast style during active pursuit (Fig. 2.2C). The average maximum speed during the burst phase was 6.3 cm s^{-1} and exponentially decreased during the coast phase to values below 1 cm s^{-1}, a nearly six-fold decrease. The decrease in speed occurred over the duration of the coast phase, which had a median value of 0.31 sec. During the burst phase, the predator accelerated and turned toward the prey with a single tail beat, which was characterized by large lateral excursions of the caudal fin. The maximum lateral

excursion of the tail was tightly correlated with the change in heading ($\Delta\theta$) during a tail beat (Fig. 2.3B).

We measured the bearing angle through time to determine the predator's pursuit strategy. Since the predator swam intermittently, our analysis focused on the burst phase where changes in heading were observed. The bearing angle immediately before a prey-oriented turn ϕ_{pre} was found to predict the change in heading of the turning maneuver (Fig. 2.3A). In contrast, we found no correlation between the measured bearing angle and the expected bearing for an interception strategy. The mean absolute bearing angle after a turning maneuver was $\phi_{\mu} = 20\,^{\circ}$, which implies some degree of inaccuracy. The slope of the regression line for $\Delta\theta$ versus ϕ_{pre} ($m = 0.71$) suggests that the predator undershot its target. This could be due to sensory limitations or may be a strategic component of the pursuit behavior. Larval zebrafish have been shown to approach targets in a series of bouts, similar to the bursts of our predators, and their successive maneuvers become more accurate (Bianco et al., 2011).

To further investigate how the bearing angle affects the control of locomotion toward prey, we developed a model to simulate a predator during active pursuit. We used classical aerodynamic models for lift and drag to compute the forces generated by the caudal fin. Our modeling approach was adapted from the robotics literature on fish-like swimmers. Dynamic models are often used by robotics researchers to develop control algorithms for their robotic fish (Morgansen et al., 2001; Wang et al., 2015, e.g.,). In contrast, our aim was to test the role of the caudal fin during turning maneuvers. Our model did not reproduce the experimentally established relationship between change in heading and tail angle (Fig. 2.3A). Instead, the simulated change in heading was minimal (results not shown). This result indicates that our model may be neglecting critical aspects of the fluid dynamics, in particular the explicit accounting of fluid-solid interactions (Fauci and Peskin, 1988; Borazjani, 2015). Another implication is that zebrafish do not rely solely on their caudal fin

to generate turning maneuvers. The pectoral and paired fins are likely important contributors and regulators of turning moments that facilitate maneuvering in zebrafish as has been shown for other species of fish (Drucker and Lauder, 2003; Fish and Lauder, 2017). Preliminary results from flow visualization (using digital particle image velocimetry) during turning maneuvers suggests that the motion of the rigid head region contributes momentum to execute turning maneuvers (see Chapter 3 Fig. 3.3 for preliminary results).

The direct relationship between the change in heading during a prey-oriented turn and the bearing angle immediately preceding the turn suggests an enhanced role of vision in this behavior. The prey's position within the predator's visual field is a critical source of sensory information that informs the predator's subsequent motor command. Since locomotion is the product of information processing (Cowan et al., 2014), we gain insight into the behavioral algorithms implemented by the neural controller of fish by assessing their pursuit kinematics. The prey-oriented turning maneuvers appear to be under feed-forward control since we did not observe the predator correct their heading during maneuvers in which the prey swam to a new position.

Our findings in the present study are limited to zebrafish predators in pursuit of evasive fish prey. It is likely that our zebrafish predators would adopt a different pursuit strategy in response to different prey items. Indeed, humans have been shown to pursue a slow moving target with a pure pursuit strategy, but adopt an interception strategy when the target moves at a sufficiently high speed (Fajen and Warren, 2007). Raptors use a mixed strategy when pursuing their prey (Kane et al., 2015). During the initial approach they use a parallel navigation strategy and switch to pure pursuit toward the end of the chase. Owls use pure pursuit during their approach to a stationary perch but use an interception strategy to pursue mice (Shifferman and Eilam, 2004). These examples demonstrate that organisms are capable of implementing a variety of pursuit strategies and the choice is context dependent.

Our predator-prey system offers the opportunity for novel research in robotics research aimed at understanding the underlying control algorithms of intermittent locomotion. Interest in the design of efficient and maneuverable underwater robotic swimmers has been growing since the advent of fish-like robots such as Robotuna (Barrett et al., 1996). Robotics engineers are increasingly looking to biology for inspiration and are collaborating with organismal biologists to understand the mechanics of locomotion (Gravish and Lauder, 2018). Intermittent locomotion is an efficient mode of travel (Paoletti and Mahadevan, 2014) and, as we have demonstrated, can be an effective strategy to pursue prey. We see the potential for biologists, engineers, and mathematicians to engage in interdisciplinary research aimed at understanding the mechanics of intermittent locomotion during goal directed behavior and applying this knowledge to design more efficient and agile robots.

2.5 Figures

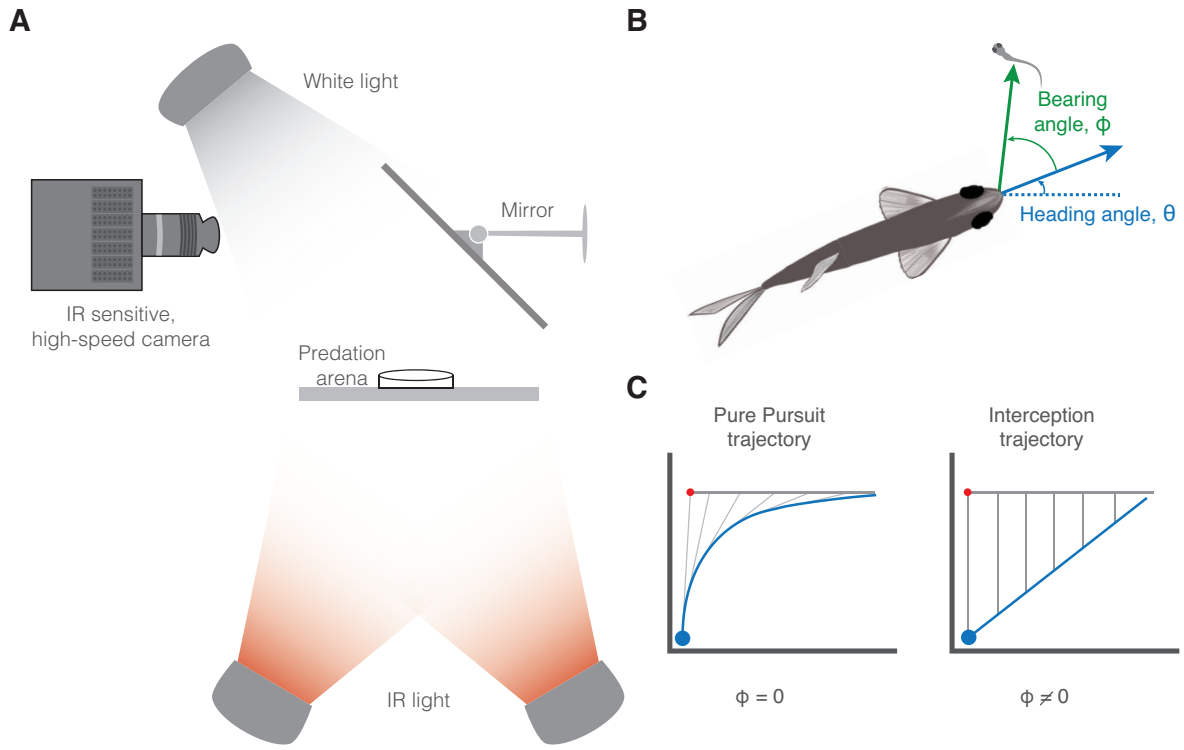

Figure 2.1: Experimental setup and pursuit strategy definitions. (A) Chase sequences were filmed from a dorsal perspective with an infrared sensitive, high-speed camera. Infrared lights provided transmitted illumination from below. A visible light source (white light) was used to provide ambient lighting. (B) The predator's heading angle (θ) is defined relative to the horizontal axis and the bearing angle (ϕ) is defined with respect to heading. Here the bearing angle is positive. (C) Hypothetical pursuit trajectories on a 2D plane for pure pursuit (left) and interception (right) for non-evasive prey. The red dot is the prey's initial position and the gray curve is its trajectory through time. The blue dot is the predator's initial position and the blue curve is its pursuit trajectory through time.

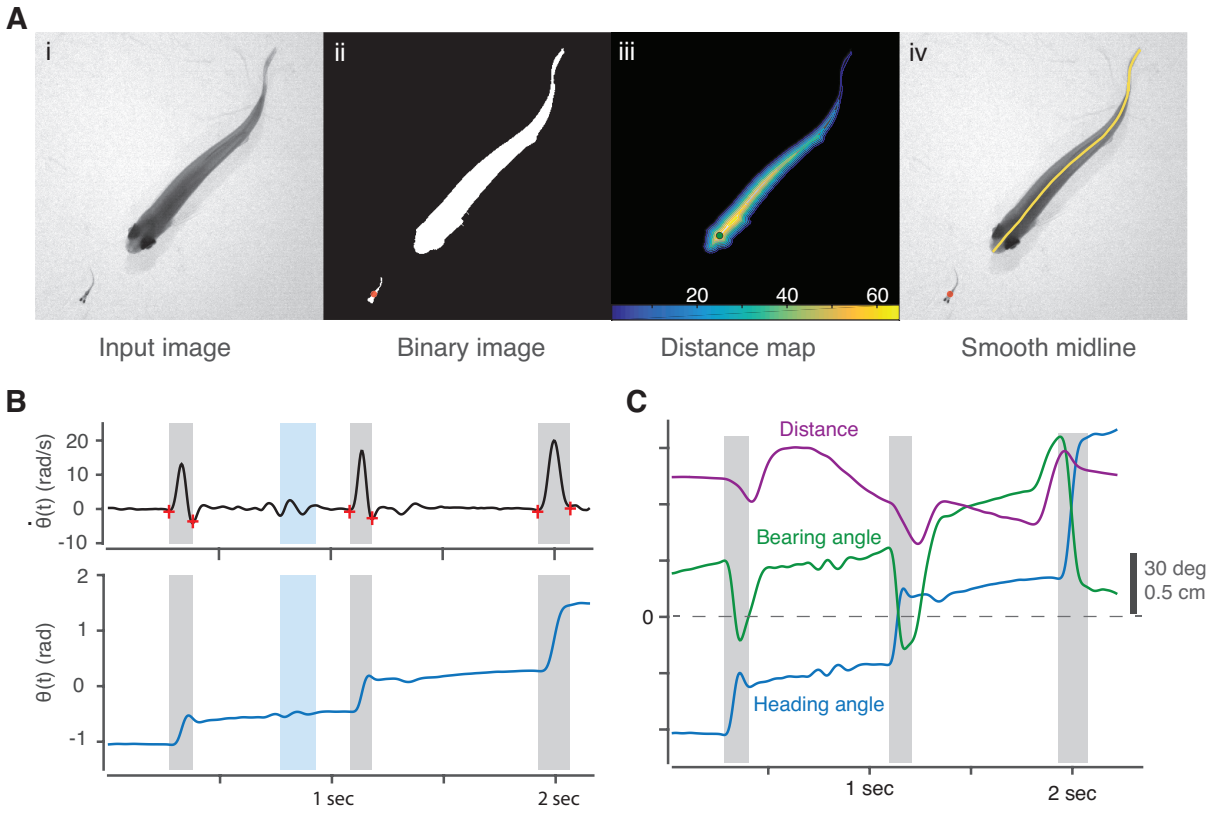

Figure 2.2: Image processing and the kinematics of pursuit in zebrafish. (A) We used image processing to extract the position of the prey (red dot in ii. and iv.) and the midline of the predator. Input images (i.), cropped for clarity, are binarized for blob analysis (ii.). The predator and prey are identified by the size of the binary blob that describes its shape. Distance mapping (iii.) is applied to the predator blob to identify the pixels that define the body midline (yellow curve in iv.). The color bar (iii.) indicates the value assigned to pixels of the predator blob based on its distance (in pixels) to the background. (B) We used features of the predator's angular velocity ($\dot{\theta}$), to identify the tail beat phases in the predator's motion. Red crosses indicate the start and end time points of a tail beat. Intervals in which the angular velocity did not meet the threshold criteria were rejected (blue bar) and intervals that achieved the threshold value were labeled as tail beat intervals (gray bars). The tail beat intervals correspond to turning maneuvers with substantial changes in the predator's heading (θ). (C) Sample time series of distance between predator and prey (purple), bearing angle (green), and heading angle (blue). The gray bars highlight the tail beat or burst phase of burst–and–coast swimming where the predator accelerates and changes heading.

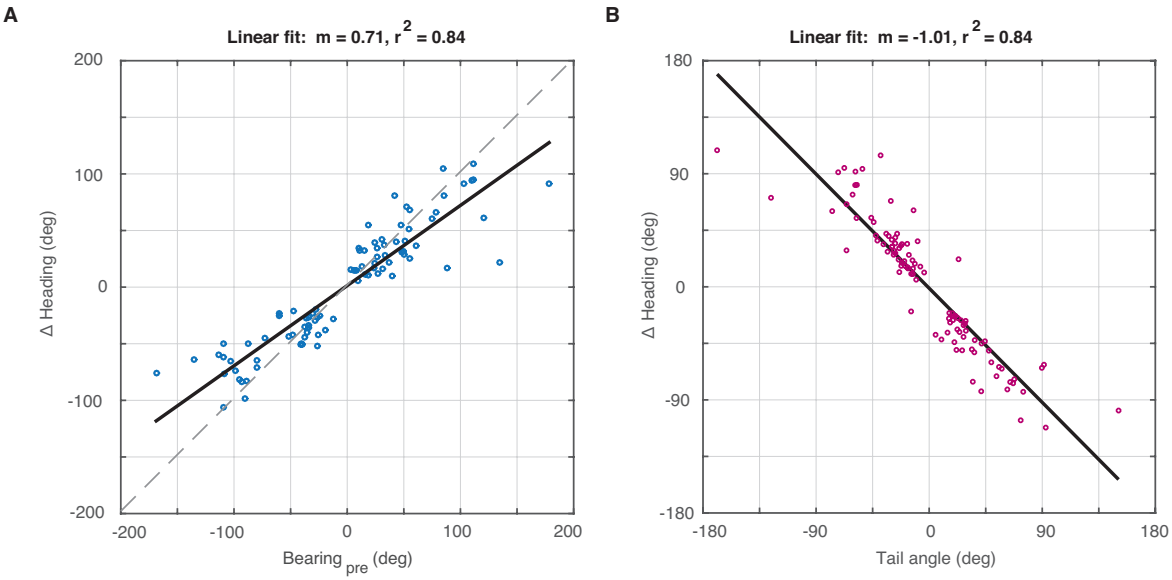

Figure 2.3: Heading change is predicted by bearing angle and correlated to tail motion. (A) The change in heading angle during a turning maneuver is predicted by the bearing angle before the turn is initiated. The slope of the regression line indicates that predator's turn toward prey to null the bearing angle, typical of a pure pursuit strategy. (B) The change in heading during a turning maneuver is correlated to the tail angle, measured as the angular deviation between the predator's heading and the position of the caudal peduncle. The slope of the regression line indicates that the predator modulates its turn amplitude by controlling the motion of its caudal fin.

Chapter 3

Multichannel Stroboscopic Videography (MSV)

Abstract

Biologists commonly visualize different features of an organism using distinct sources of illumination. Multichannel imaging has largely not been applied to behavioral studies due to the challenges posed by a moving subject. We address this challenge with the technique of Multichannel Stroboscopic Videography (MSV), which synchronizes multiple strobe lights with video exposures of a single camera. We illustrate the utility of this approach with kinematic measurements of a walking cockroach (*Gromphadorhina portentosa*) and calculations of the pressure field around a swimming fish (*Danio rerio*). In both, transmitted illumination generated high-contrast images of the animal's body in one channel. Other sources of illumination were used to visualize the points of contact for the feet of the cockroach and water flow around the fish in separate channels. MSV provides an enhanced

potential for high-throughput experimentation and the capacity to integrate changes in physiological or environmental conditions in freely-behaving animals.

3.1 Introduction

The visualization of multiple channels of spatial information is common to numerous fields of biological study. Multichannel visualization is often associated with fluorescence microscopy, where distinct channels may be recorded by using different fluorophores (e.g. Parak et al., 2005; Miyawaki et al., 2003; Carlsson et al., 1994). Individual channels are visualized with a single camera by changing the filter sets in a light path that are specific to each fluorophore. Overlaying these channels into a single image provides the ability to map disparate types of information offered by each channel (e.g. gene expression, ion concentration, mechanical stresses) with respect to an organism's body. In this way, multichannel visualization provides a powerful means for experimental inquiry. However, the leverage gained by a multichannel approach has largely eluded studies of animal behavior due to the relatively rapid motion of the subject. Here we present a technique called Multichannel Stroboscopic Videography (MSV) that permits multichannel visualization for behavioral experiments with a single camera. MSV operates through the use of strobe lights that are synchronized with respect to the exposures of a video camera. Each set of lights provides illumination that is specific to an individual channel in a recording. Channels are recorded during distinct video frame exposures. We illustrate the utility of this technique by measuring (1) two channels of kinematic data in a walking cockroach and (2) the flow field and kinematics in separate channels for a swimming zebrafish.

Our measurements of a walking cockroach were intended to demonstrate the general approach and value of MSV for automated kinematic analysis. Cockroaches are a model system for the neuromechanics of locomotion and studies on this insect can include simultaneous measurements of the animal's body and where its feet contact the ground (Kram et al., 1997; Schaefer and Ritzmann, 2001; Watson and Ritzmann, 1997; Full and Tu, 1990) that are acquired by established methods. As detailed in Materials and methods, we used

MSV to independently optimize the illumination of the body in one channel and the feet in another. The contrast for both the body and feet were sufficient to automate the acquisition of coordinates for both features without the use of synthetic markers. This approach could be applied to other such situations where two or more sources of illumination provide high contrast for distinct features of an organism. Automated kinematic analysis allows for high-throughput behavioral experimentation.

Our experiment on a swimming zebrafish was designed to evaluate the use of MSV to generate two distinct types of data. One channel recorded the flow field around the fish using digital particle image velocimetry (DPIV) and the other tracked the peripheral shape of the body. In addition to the benefits of correlating measurements from the two channels, measurements of the fish's body were also incorporated in our analysis of DPIV data. In particular, automated tracking of the body allowed for the definition of a dynamic mask to reject erroneous velocity vectors. In addition, the position of the fluid-body interface was necessary to calculate the pressure field using a previously described method (Lucas et al., 2017; Dabiri et al., 2014). The ability to automate measurements of both the animal's body and flow field illustrates MSV's powerful capacity for high-throughput experimentation with a complex hydrodynamic analysis.

3.2 Materials and methods

3.2.1 Experiments

MSV requires an ability to synchronize sources of stroboscopic illumination with respect to the frame exposures of a video camera. We used a high-speed video camera (FASTCAM Mini AX100, Photron, San Diego, CA, USA) with high spatial resolution (1024×1024 pixels) configured with a macro lens (Micro-Nikkor 105 mm $f/2.8$, Nikon Inc., Melville,

NY, USA), appropriate for recording small animals (Fig. 3.1). This camera was configured to have the timing of exposures dictated by the rising edge of an external 5 V square-wave control signal of variable frequency. This signal was provided by a 2-channel arbitrary waveform function generator (DG1022Z, RIGOL Technologies, Beaverton, OR, USA), which also generated a second 5 V control signal for the lights at half the frequency of the camera's control signal. The signals used to operate the camera and light sources were synchronized using the 'align-phase' feature of the function generator and verified with a multi-channel digital oscilloscope (DS1054Z, RIGOL Technologies, Beaverton, OR, USA). When recording at high speed, MSV requires lights such as LEDs that have a nearly instantaneous response to a power control signal. A consequence of MSV is that the different channels generate measurements that are separated in time, which requires interpolating the data in post-processing (explained below).

We used MSV to measure the kinematics of the body and feet of a cockroach in separate channels. To visualize the body, we used an infrared (IR, 940 nm) LED panel placed above a translucent white acrylic diffuser, which was placed above the experimental tank (Fig. 3.1A). This generated a high-contrast image of the body with transmitted illumination. A circuit (Fig. S1) delivered power to this light when a control signal was set to 0 V and no power at 5 V. We visualized where the feet of the cockroach contacted the floor of the tank using a second light that consisted of a strip of white LEDs aligned with the edge of the floor. The floor was composed of a clear sheet of acrylic (30.5 cm × 30.5 cm × 1.3 cm) and the strip of LEDs generated an evanescent field by partial total internal reflection (Martin-Fernandez et al., 2013) above the acrylic surface. When the legs of the cockroach contacted the surface, light within the evanescent field was reflected and imaged from below. The strip of white LEDs was powered throughout the experiment, but their low brightness was barely visible when the IR light source was activated to visualize the cockroach's body. As

a consequence, video recordings consisted of alternating high-contrast images suitable for automating the body and footfall kinematics of a walking cockroach in separate channels.

Our experimental setup for zebrafish allowed for simultaneous recordings of the fish's body and the surrounding flow field. The body was visualized with the same IR LED panel and diffuser (Fig. 3.1B) as used for the cockroach experiment. The IR LED panel was oriented below the experimental tank (7.5 cm × 7.5 cm) and the camera was placed above to visualize the fish as a high-contrast silhouette from a dorsal perspective. We visualized flow by splitting a laser beam (2 W DPSS, 532 nm wavelength, Laser Quantum, San Jose, CA, USA) into two light paths, one of which was reflected upon two mirrors, and passing each path through sheet generator optics (Fig. 3.1B). This arrangement generated a plane of light parallel to the focal plane of the camera from two perpendicular sources. The laser sheet illuminated reflective particles (industrial diamond powder, $3-6\,\mu$m, Lasco Diamond Products, Chatsworth, CA, USA) mixed at a concentration of 0.0056% by weight in the water contained within the tank, which was filled to a depth of 2.5 cm.

The two different single-wavelength light sources used in our fish experiments created a chromatic aberration. Most lenses have different refractive indices for different wavelengths of light. As a consequence, a lens focused on a subject for one color will be out of focus for a different color. Due to this effect, we optimized the setup for increased depth-of-field by increasing the intensity of the IR LED panel and the gain on the camera so that we could set the lens with a higher f-number and hence smaller aperture. In addition, we focused our lens on the laser sheet because DPIV results were found to be more sensitive to focus.

The fish's body and flow field were independently recorded at high speed (Fig. 3.2). The IR LED panel and laser received a common 500 Hz control signal from the function generator. We modified the external control hardware of the laser to emit only when this signal reached 5 V. In contrast, the IR LED panel emitted light at 0 V and hence out of phase with the

laser. The other channel from the function generator synchronized frame exposures with a 1000 Hz control signal. Thus two channels of alternating video frames were recorded for dynamic boundary tracking and flow visualization.

Experiments were performed on a single fish and one cockroach. The zebrafish (*Danio rerio*, Hamilton 1822, 120 days post-fertilization, 18.9 mm standard length) was maintained in a recirculating freshwater system at 27 °C on a 14 L:10 D cycle. The cockroach (*Gromphadorhina portentosa*, 6.83 g) was obtained from a laboratory colony maintained at 24 °C under a 12 L:12 D cycle. Both animals were transferred to their experimental tank and allowed to acclimate for at least 10 min prior to filming. Spontaneous behavior was recorded for both animals. For the fish, we stopped recording and saved the sequence to disk when the animal executed a turning maneuver within the horizontal plane of the laser sheet. All experiments on the fish were conducted in accordance with the University of California, Irvine's Institutional Animal Care and Use Committee (Protocol #AUP-17-012).

3.2.2 Image processing and data analysis

Our recordings of the cockroach were analyzed to automate tracking of both the body and feet. This procedure, and all data analyses, were performed by programming within MATLAB (v.2014b, MathWorks, Natick, MA, USA). Our program employed the image processing task generally known as blob analysis which requires the conversion of grayscale images into binary images by defining an intensity value that separates dark and light pixels. This image segmentation technique, known as thresholding, generates 'blobs' of connected pixels from which features (e.g. centroid and area) may be calculated. The program first identified the frames for the body by the relatively high mean pixel intensity generated by the IR LED panel (Fig. 3.3A). This initial detection procedure allowed us to input the entire video without imposing a specific ordering to the frames and without

manually separating frames into subdirectories. After thresholding, the cockroach's body was distinguished as the largest blob in each frame and its centroid position was recorded. We performed a similar operation to identify the illuminated points of contact for the feet from the darker video frames. The more subtle contrast of these images was improved by subtracting a time-averaged image to remove imperfections in the surface of the floor. We combined the coordinates from both channels by linear interpolation ('interp1' function in Matlab) of the body position coordinates at the same time points for which we obtained measurements of the feet. The final result was a kinematic dataset for the body and feet that was obtained automatically through two channels.

One of the channels for our fish experiments similarly allowed for body tracking. Our program automatically tracked the boundary and midline of the dark fish body from the video frames illuminated by IR light (Fig. 3.3B). We applied a local thresholding technique ('adaptthresh' function in MATLAB) that is robust to nonuniform illumination and can be used with or, as implemented here, without an input reference image for background subtraction. The resulting binary image described the shape of the fish's body, which we refined with morphological operations to fill holes and connect any gaps with neighboring blobs. The fish blob was manually selected in the first video frame and subsequently identified by its area and proximity to the prior frame's blob. This blob was used as our dynamic mask for DPIV analysis and served as the basis for kinematic measurements. For each frame, we measured the blob's area and identified its center-of-area, boundary, and midline. The midline was identified by distance mapping, which encodes a value for each pixel according to its closest proximity to the blob's edge. We applied distance mapping along the rows and columns of the binary image and the resulting maps were concatenated to produce the set of pixels that define the midline (Fig. 3.3B, right column). For kinematic analysis, the raw midline coordinates were smoothed with the 'loess' method, a locally weighted polynomial regression.

The DPIV flow fields were analyzed to estimate the pressure field around the swimming fish (Figs. 3.3C and S2). We analyzed our recordings of particle motion using an open-source MATLAB application PIVlab (Thielicke and Stamhuis, 2014). This software was configured for a direct Fourier transform correlation with three passes and 50% window overlap. We decreased the interrogation window sizes (64×64, 32×32, and 16×16) in each pass, which resulted in a 128×128–velocity vector field. We modified PIVlab to accept the dynamic mask that we identified from our blob analysis (Fig. 3.3B). A linear interpolation of the flow fields with respect to time was performed to estimate the flow field for the same instants of time for which we recored body kinematics. Pressure calculations were performed with the queen2 algorithm (Dabiri et al., 2014) with default settings. This algorithm directly computed the pressure gradient term in the Navier-Stokes equations along several paths and performed a median-polling scheme to estimate the pressure at each point. These calculations required the coordinates of the mask boundary for the fish's body from each frame.

3.3 Results and discussion

Our experiments illustrate how MSV allows multichannel visualization for behavioral experiments. Channels of data were obtained from images of alternating sources of illumination in a single-camera video recording. The two channels of kinematics in our cockroach experiment were acquired from images that individually visualized the footfall pattern and body position through time (Fig. 3.3A). In our fish experiment, flow was visualized with a DPIV channel and kinematics were obtained through another channel. This kinematics channel was then used in the post-processing of the DPIV channel (Fig. 3.3B-C). We see the potential for broad applications of MSV in the study of animal behavior and engineering research.

MSV can enhance the automated acquisition of kinematic measurements. Automated analyses allow high-throughput data acquisition that is useful for expanding the size of a dataset and may facilitate applications such as behavioral mutant screens (e.g. Brockerhoff et al., 1995; Mirat et al., 2013). Machine learning and other frontiers in image processing offer opportunities for the development of sophisticated software for automating kinematic measurements (Colyer et al., 2018; Robie et al., 2017). However, a more direct and robust approach to automation may be obtained from video recordings of subjects that are illuminated with high contrast. Under two or more sources of illumination, each source may be optimized to enhance the contrast of a particular feature. In the case of the cockroach, the lighting conditions for the body and feet were optimized independently (Fig. 3.3A). Recording over two channels allowed these features to be visualized with sufficient contrast for automated tracking. This example demonstrates the value of MSV in allowing landmark tracking under two or more sources of illumination, which may be required in animal behavior research for which automated tracking methods are not well established. MSV could be extended to tracking multiple individuals in an experiment. For example, individuals marked with a UV fluorescent tag (Delcourt et al., 2013, 2011) could be identified under UV illumination in one channel and body kinematics could be recorded via transmitted illumination in another channel.

Our fish experiment demonstrates the utility of MSV in measuring flow around a moving body. DPIV operates by identifying the displacement of particles within an Eulerian system grid (Stamhuis et al., 2002; Adrian, 1991). Excluding the cells within an interrogation window that contain a body may be accomplished by dynamic masking. Dynamic masks may be isolated with image processing from a single-channel recording when the body is uniformly illuminated (Gemmell et al., 2016), but the lighting conditions that are amenable to recording particles are generally unfavorable for visualizing the body. As a consequence, the body is often manually drawn for each frame of the video (Gemmell et al., 2016; Tytell

and Lauder, 2004), which is labor-intensive. As demonstrated presently, MSV provides the opportunity to resolve this challenge by producing images of the moving body under transmitted illumination that may be easily converted into a dynamic binary mask. This automated process has the potential for utility beyond biology and into areas of fluid dynamics research. When imaging a moving subject in flow, MSV can be used in place of image processing techniques for masking that require *a priori* descriptions of the object's geometry and motion (e.g. Nikoueeyan and Naughton, 2018; Dussol et al., 2016). As an alternative to MSV, it is possible to use two sources of illumination and multiple cameras to simultaneously acquire the different channels (Adhikari et al., 2015). However, such a system results in higher cost and greater computational time for image registration of the different camera views relative to MSV.

MSV offers additional benefits in the post-processing of flow measurements for near-field analysis. After acquiring a velocity field, investigators are generally interested in extracting derived features from those data. Such post-processing has included measurements of variables describing the circulation and spacing of vortices shed in the wake of an animal (Drucker and Lauder, 2001; Müller et al., 2000). When conducted in the far field, such calculations may not require articulating the location of the body's surface. However, the body's boundaries are essential for calculating near-field phenomena, such as boundary layers and flow separation (Anderson et al., 2001). Measurements of the surface in these cases offers the same challenge as the dynamic mask used in acquisition. Again, MSV resolves this task by allowing for the automated extraction of a body's boundary in the flow field, as demonstrated in our calculation of pressure (Fig. 3.3C). The algorithm that we used, developed previously (Lucas et al., 2017; Dabiri et al., 2014), required identifying the boundary of the fish for each video frame.

There are limitations to MSV that are a direct consequence of using a single camera to collect multi-channel data. Consecutive images from a single light source (Fig. 3.2C)

are offset by an inter-frame interval equal to the camera's frame rate, which effectively reduces the frame rate by half. This drop in frame rate can be ameliorated, to some extent, by using a high speed video camera and sufficient lighting to illuminate the object as exposure time decreases. Another potential drawback is that MSV does not generate simultaneous multi-channel data. Many biological investigations benefit from correlating simultaneous data from multiple sources (e.g. Venkatraman et al., 2010; Mead et al., 2003). The high temporal resolution of our data allowed for interpolating the data of one channel at corresponding time points of the second channel. Similar post-processing is required to synchronize measurements from different channels.

The ability of MSV to acquire multiple channels of image data has potential applications in diverse areas of biological research. Multichannel visualization is common to fluorescence microscopy, where distinct channels may be imaged with different fluorophores (e.g. Parak et al., 2005; Miyawaki et al., 2003; Carlsson et al., 1994). Each fluorophore, visualized with a distinct filter set, can offer a channel that maps a type of information (e.g. gene expression, ion concentration, mechanical stresses) to an organism's anatomy and these channels may be combined in a single image. The use of transgenic lines of animals for the visualization of neuronal activity has become a popular optical approach to neurophysiology but generally requires a stationary subject (e.g. Bruegmann et al., 2015; McLean and Fetcho, 2011). Using independent frame exposures, MSV may permit visualization of tissues in a moving subject by combining a fluorescence channel with another light source to visualize the body.

In summary, MSV offers the opportunity for multichannel visualization with a moving subject. By separating the channels in separate exposures of a video recording, the illumination for each channel may be optimized for a particular source of information. Such conditions offer the promise of automated analysis and sophisticated post-processing. We feel that the cockroach and fish experiments presented here illustrate just some of the pos-

sibilities for incorporating this approach in experimental methods for research in biology and engineering.

Data accessibility

Dash UCI: https://doi.org/10.7280/D1R67V

3.4 Figures: MSV

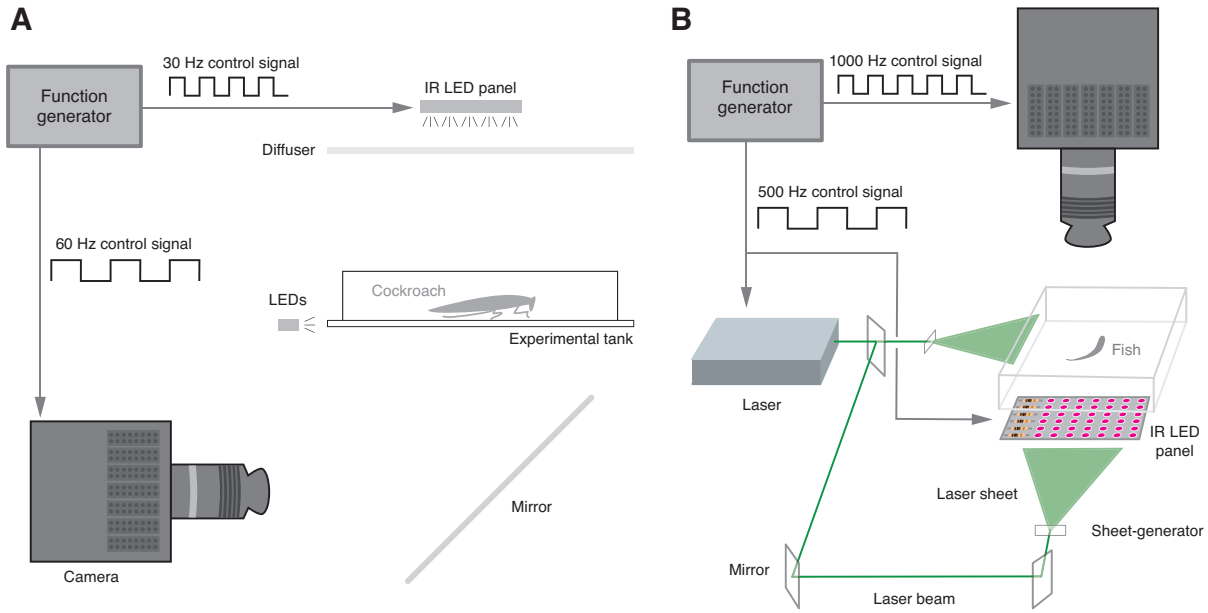

Figure 3.1: Two experimental setups that use MSV. (A) We performed an experiment on a cockroach using two channels of kinematics. Foot kinematics were obtained using LEDs directed toward the side of the acrylic floor to illuminate where the feet contacted the floor. Body kinematics were measured using an IR LED panel positioned above the animal and holding tank to visualize the body with high contrast. This panel was activated by a function generator using a control signal that was synchronized with a camera that recorded at twice the frequency. (B) We performed experiments with channels for flow visualization (via DPIV) and kinematics for a fish executing a turning maneuver. The camera recorded the motion of the fish's body under transmitted illumination using the IR LED panel and the motion of suspended reflective particles using the laser in alternating frames of video. See Fig. 3.2 for further details on the synchronization of lights and camera.

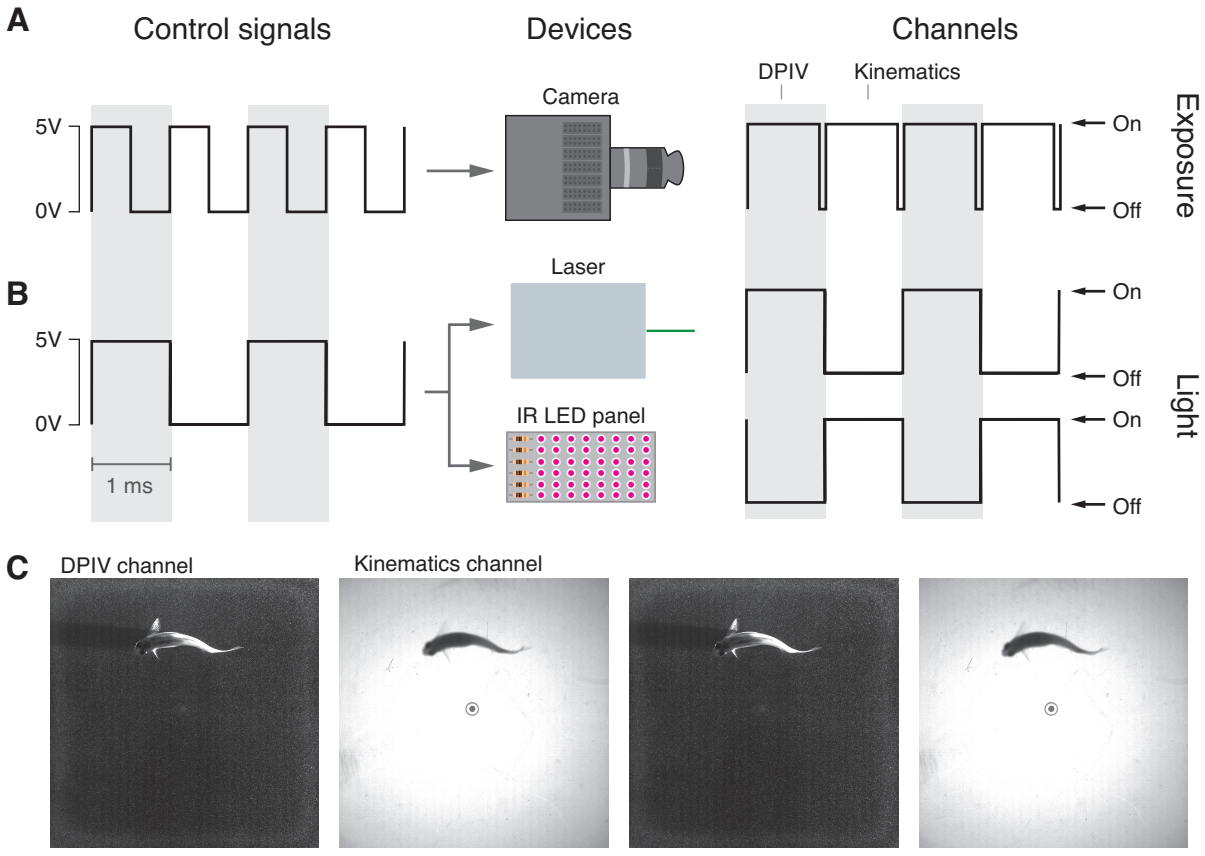

Figure 3.2: The control of light sources and camera exposures for DPIV and kinematics channels with MSV. (A) We used a square-wave signal (1000 Hz, 5 V) to control the timing of exposure for the high-speed video camera, which was configured to respond to the leading edge of the signal. (B) A second signal from the function generator that generated the camera signal (Fig. 3.1) was output to control hardware for the laser and IR LED panel. This square-wave was in-phase with the camera signal, but at half the frequency (500 Hz, 5 V). The control hardware for the laser was configured to turn 'On' in response to a 5 V signal, whereas the IR LED panel had the opposite response. As a consequence, the two sources emitted light out of phase and were captured on different frame exposures. (C) Using this method, sample images were acquired of an adult zebrafish from a dorsal view as it executed a turn at 1 ms intervals alternating between the two channels. The DPIV channel illuminated suspended particles with laser light (see Fig. S2B) and the kinematics channel used the IR LED panel for transmitted illumination.

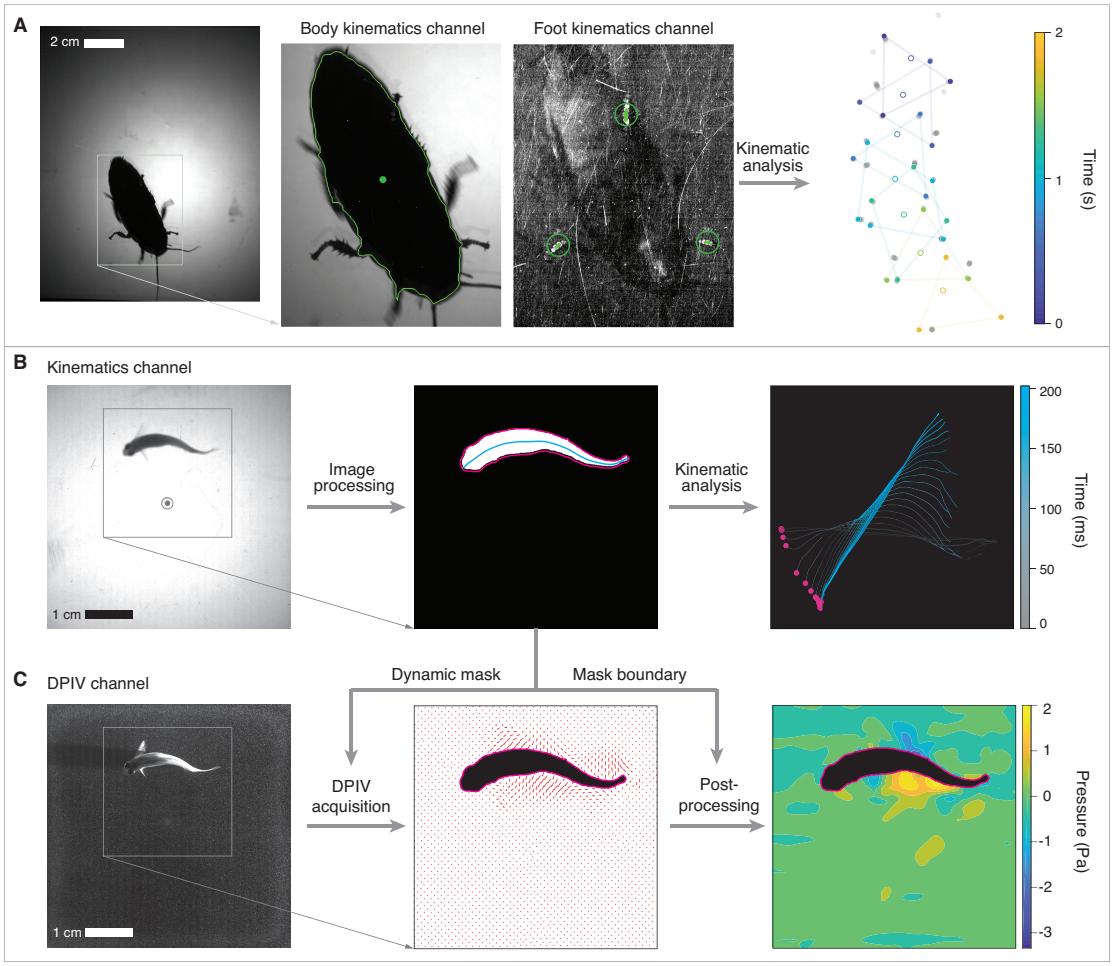

Figure 3.3: Workflow of MSV analysis for experiments on a (A) cockroach and (B–C) fish. (A) Cockroach motion was measured using body kinematics and foot kinematics channels. An individual video frame (left) shows the body under transmitted illumination from which the center-of-area of the body (green circle in inset) was obtained by automated image processing. The position of the center of three contact points for the feet (green circles) are shown for the foot kinematics channel (frame is contrast-enhanced). By interpolating the body position, we combined measurements of the center of body (open circles) and points of contact for the feet (filled circles) for the same point in time (connected by lines at 0.32 s intervals). The contact points of other times (in gray) are shown as well. (B) A video frame of a zebrafish executing a turning maneuver (left column) was automatically processed to extract the object mask, boundary, and midline (center column). By analyzing a sequence of frames (right column), the midlines (in blue) and rostrum (in magenta) are shown for a 200 ms counterclockwise turn to demonstrate an automated analysis conducted from the kinematics channel. (C) A video frame from the DPIV channel displays the particles around the zebrafish. From a pair of such images, the velocity field was calculated (center column) using a dynamic binary mask for the body from the kinematics channel. A pressure field was calculated (right column) by post-processing of the velocity field using the mask boundary from the kinematics channel.

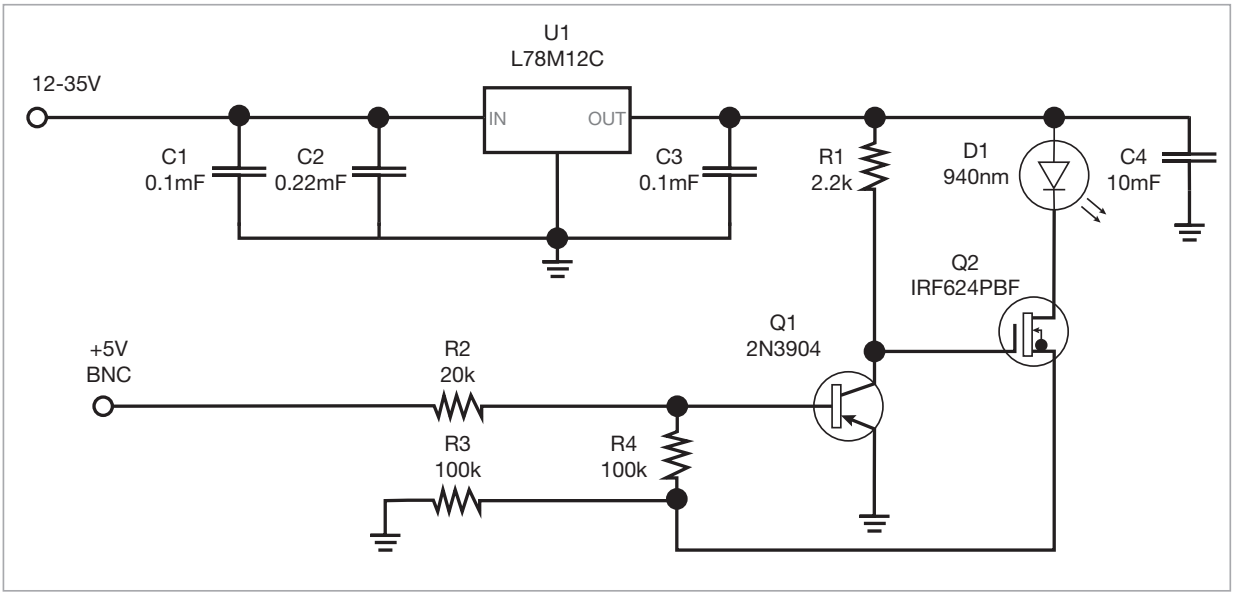

Figure 3.4: Circuit diagram to power IR LEDs. The IR LEDs are powered by a 12-35 V input and may be switched off by supplying a 5 V input control signal.

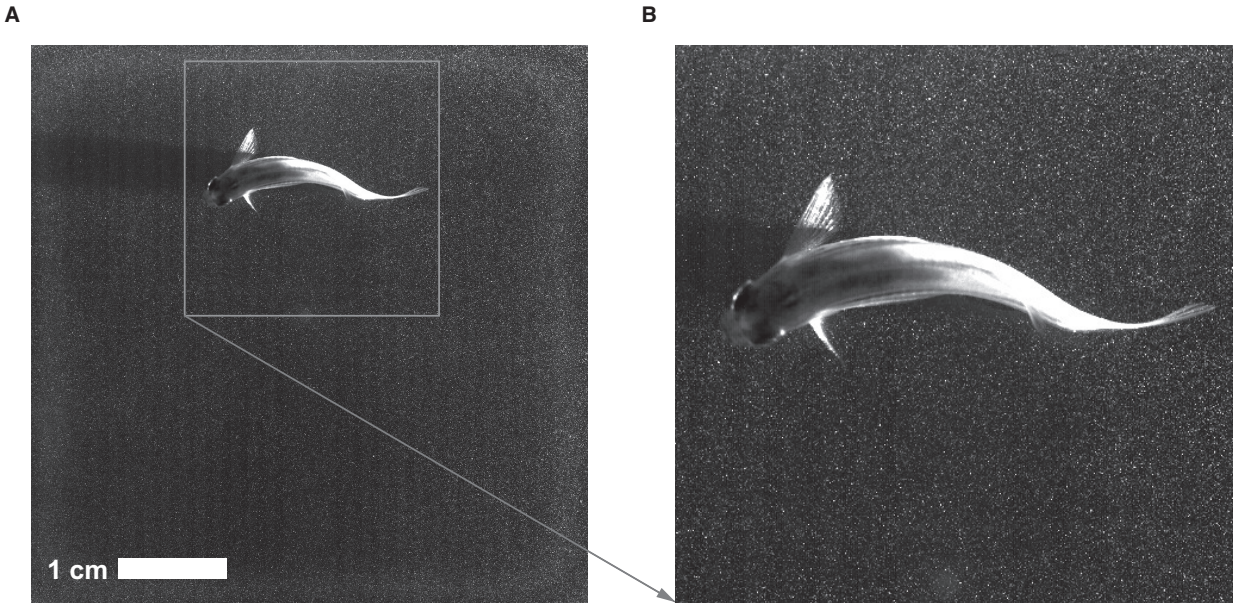

Figure 3.5: DPIV image of zebrafish (A) and inset (B). (A) Full frame DPIV image (1024×1024 pixels) of zebrafish during a turning maneuver. (B) Inset showing the fish body and laser illuminated particles around the fish body.

Bibliography

Adhikari, D., Gemmell, B. J., Hallberg, M. P., Longmire, E. K. and Buskey, E. J. (2015). Simultaneous measurement of 3D zooplankton trajectories and surrounding fluid velocity field in complex flows. *J. Exp. Biol.* **218**, 3534–3540.

Adrian, R. J. (1991). Particle-imaging techniques for experimental fluid mechanics. *Annual Rev. Fluid Mech.* **23**, 261–304.

Aliprantis, C. D. and Chakrabarti, S. K. (2011). *Games and Decision Making*. Oxford University Press, USA.

Alpern, S., Fokkink, R., Timmer, M. and Casas, J. (2011). Ambush frequency should increase over time during optimal predator search for prey. *Journal of the Royal Society Interface* **8**, 1665–1672.

Anderson, E., McGillis, W. and Grosenbaugh, M. (2001). The boundary layer of swimming fish. *J. Exp. Biol.* **204**, 81–102.

Arnott, S. A., Neil, D. M. and Ansell, A. D. (1999). Escape trajectories of the brown shrimp *Crangon crangon*, and a theoretical consideration of initial escape angles from predators. *J. Exp. Biol.* **202**, 193–209.

Bainbridge, R. (1958). The Speed of Swimming of Fish as Related to Size and to the Frequency and Amplitude of the Tail Beat. *J. Exp. Biol* **35**, 109–133.

Bardi, M., Falcone, M. and Soravia, P. (1999). Numerical Methods for Pursuit-Evasion Games via Viscosity Solutions. In *Stochastic and Differential Games*, pp. 105–175. Boston, MA: Birkhäuser Boston.

Barrett, D., Grosenbaugh, M. and Triantafyllou, M. (1996). The optimal control of a flexible hull robotic undersea vehicle propelled by an oscillating foil. *IEEE* .

Bianco, I. H., Kampff, A. R. and Engert, F. (2011). Prey capture behavior evoked by simple visual stimuli in larval zebrafish. *Front. in Syst. Neuro.* **5**, 101.

Borazjani, I. (2015). Simulations of Unsteady Aquatic Locomotion: From Unsteadiness in Straight-Line Swimming to Fast-Starts. *Integr. Comp. Biol.* **55**, 740–752.

Borazjani, I. and Sotiropoulos, F. (2008). Numerical investigation of the hydrodynamics of carangiform swimming in the transitional and inertial flow regimes. *J. Exp. Biol.* **211**, 1541–1558.

Briggs, J. P. (2002). The zebrafish: A new model organism for integrative physiology. *Am. J. Physiol. Regulatory Integrative Comp. Physiol* **282**, R3–R9.

Brighton, C. H., Thomas, A. L. R. and Taylor, G. K. (2017). Terminal attack trajectories of peregrine falcons are described by the proportional navigation guidance law of missiles. *Proc. Natl Acad. Sci USA* **114**, 13495–13500.

Brockerhoff, S. E., Hurley, J. B., Janssen-Bienhold, U., Neuhauss, S. C., Driever, W. and Dowling, J. E. (1995). A behavioral screen for isolating zebrafish mutants with visual system defects. *Proc. Natl. Acad. Sci. U.S.A.* **92**, 10545–10549.

Bruegmann, T., van Bremen, T., Vogt, C. C., Send, T., Fleischmann, B. K. and Sasse, P. (2015). Optogenetic control of contractile function in skeletal muscle. *Nat. Commun.* **6**, 7153.

Budick, S. A. and O'Malley, D. M. (2000). Locomotor repertoire of the larval zebrafish: Swimming, turning and prey capture. *J. Exp. Biol.* **203**, 2565–2579.

Card, G. and Dickinson, M. H. (2008). Visually mediated motor planning in the escape response of Drosophila. *Current Biology* **18**, 1300–1307.

Carlsson, K., Aslund, N., Mossberg, K. and Philip, J. (1994). Simultaneous confocal recording of multiple fluorescent labels with improved channel separation. *J. Microscopy* **176**, 287–299.

Casas, J. and Steinmann, T. (2014). Predator-induced flow disturbances alert prey, from the onset of an attack. *Proceedings. Biological sciences / The Royal Society* **281**, 20141083–20141083.

Catania, K. C. (2009). Tentacled snakes turn C-starts to their advantage and predict future prey behavior. *Proceedings of the National Academy of Sciences* **106**, 11183–11187.

Chiu, C., Reddy, P. V., Xian, W., Krishnaprasad, P. S. and Moss, C. F. (2010). Effects of competitive prey capture on flight behavior and sonar beam pattern in paired big brown bats, Eptesicus fuscus. *J. Exp. Biol.* **213**, 3348–3356.

Collett, T. S. and Land, M. F. (1978). How Hoverflies Compute Interception Courses. *Journal of Comparative Physiology* **125**, 191–204.

Colyer, S. L., Evans, M., Cosker, D. P. and Salo, A. I. T. (2018). A review of the evolution of vision-based motion analysis and the integration of advanced computer vision methods towards developing a markerless system. *Sports Med. Open* **4**, 24.

Combes, S. A., Rundle, D. E., Iwasaki, J. M. and Crall, J. D. (2012). Linking biomechanics and ecology through predator–prey interactions: flight performance of dragonflies and their prey. *J. Exp. Biol.* **215**, 903–913.

Cowan, N. J., Ankarali, M. M., Dyhr, J. P., Madhav, M. S., Roth, E., Sefati, S., Sponberg, S., Stamper, S. A., Fortune, E. S. and Daniel, T. L. (2014). Feedback Control as a Framework for Understanding Tradeoffs in Biology. *Integr. Comp. Biol.* **54**, icu050–237.

Dabiri, J. O., Bose, S., Gemmell, B. J., Colin, S. P. and Costello, J. H. (2014). An algorithm to estimate unsteady and quasi-steady pressure fields from velocity field measurements. *J. Exp. Biol* **217**, 331–6.

Delcourt, J., Denoël, M., Ylieff, M. and Poncin, P. (2013). Video multitracking of fish behaviour: a synthesis and future perspectives. *Fish and Fisheries* **14**, 186–204.

Delcourt, J., Ylieff, M., Bolliet, V., Poncin, P. and Bardonnet, A. (2011). Video tracking in the extreme: a new possibility for tracking nocturnal underwater transparent animals with fluorescent elastomer tags. *Behav. Res. Methods* **43**, 590–600.

deVries, M. S., Murphy, E. A. K. and Patek, S. N. (2012). Strike mechanics of an ambush predator: the spearing mantis shrimp. *J. Exp. Biol.* **215**, 4374–4384.

Dickinson, M. H. and Götz, K. G. (1993). Unsteady aerodynamic performance of model wings at low Reynolds numbers. *J. Exp. Biol.* **174**, 45–64.

Dickinson, M. H., Lehmann, F. O. and Sane, S. P. (1999). Wing rotation and the aerodynamic basis of insect flight. *Science* **284**, 1954–1960.

Dill, L. (1974). Escape response of zebra danio (*Brachydanio-Rerio*). 1. Stimulus for Escape. *Anim. Behav.* **22**, 711–722.

Domenici, P., Batty, R. S., Simila, T. and Ogam, E. (2000). Killer whales (*Orcinus orca*) feeding on schooling herring (*Clupea harengus*) using underwater tail-slaps: kinematic analyses of field observations. *J. Exp. Biol.* **203**, 283–294.

Domenici, P. and Blagburn, J. M. (2011a). Animal escapology I: theoretical issues and emerging trends in escape trajectories. *J. Exp. Biol.* **214**, 2463–2473.

Domenici, P. and Blagburn, J. M. (2011b). Animal escapology II: escape trajectory case studies. *J. Exp. Biol.* **214**, 2474–2494.

Domenici, P., Booth, D., Blagburn, J. M. and Bacon, J. P. (2008). Cockroaches keep predators guessing by using preferred escape trajectories. *Curr. Biol.* **18**, 1792–1796.

Drucker, E. and Lauder, G. V. (2001). Wake dynamics and fluid forces of turning maneuvers in sunfish. *J. Exp. Biol* **204**, 431–442.

Drucker, E. G. and Lauder, G. V. (2003). Function of pectoral fins in rainbow trout: behavioral repertoire and hydrodynamic forces. *Journal of Experimental Biology* **206**, 813–826.

Dussol, D., Druault, P., Mallat, B., Delacroix, S. and Germain, G. (2016). Automatic dynamic mask extraction for PIV images containing an unsteady interface, bubbles, and a moving structure. *CR Mécanique* **344**, 464–478.

Emlen, D. J. (2014). *Animal Weapons: The Evolution of Battle*. New York: Macmillan.

Evans, D. L. and Schmidt, J. O. (1990). *Insect Defenses: Adaptive Mechanisms and Strategies of Prey and Predators*. Albany, NY: SUNY Press.

Fajen, B. R. and Warren, W. H. (2007). Behavioral dynamics of intercepting a moving target. *Experimental Brain Research* **180**, 303–319.

Fauci, L. J. and Peskin, C. S. (1988). A computational model of aquatic animal locomotion. *Journal of Computational Physics* **77**, 85–108.

Fish, F. E. and Lauder, G. V. (2017). Control surfaces of aquatic vertebrates: active and passive design and function. *J. Exp. Biol.* **220**, 4351–4363.

Fuiman, L. A. (1994). The interplay of ontogeny and scaling in the interactions of fish larvae and their predators. *J. Fish Biol.* **45**, 55–79.

Full, R. J. and Tu, M. S. (1990). Mechanics of six-legged runners. *J. Exp. Biol* **148**, 129–146.

Gemmell, B. J., Fogerson, S. M., Costello, J. H., Morgan, J. R., Dabiri, J. O. and Colin, S. P. (2016). How the bending kinematics of swimming lampreys build negative pressure fields for suction thrust. *J. Exp. Biol.* **219**, 3884–3895.

Ghose, K., Horiuchi, T. K., Krishnaprasad, P. S. and Moss, C. F. (2006). Echolocating bats use a nearly time-optimal strategy to intercept prey. *Plos Biology* **4**, 865–873.

Gibbons, R. (1992). *A Primer in Game Theory*. Harverter Wheatsheaf.

Gilbert, C. (1997). Visual control of cursorial prey pursuit by tiger beetles (Cicindelidae). *Journal of Comparative Physiology a-Sensory Neural and Behavioral Physiology* **181**, 217–230.

Gravish, N. and Lauder, G. V. (2018). Robotics-inspired biology. *The J. Exp. Biol.* **221**, jeb138438.

Heuch, P. A., Doall, M. H. and Yen, J. (2007). Water flow around a fish mimic attracts a parasitic and deters a planktonic copepod. *Journal Of Plankton Research* **29**, i3–i16.

Higgs, D. and Fuiman, L. (1996). Ontogeny of visual and mechanosensory structure and function in Atlantic menhaden Brevoortia tyrannus. *J. Exp. Biol* **199**, 2619–2629.

Higham, T. E. (2007). Feeding, fins and braking maneuvers: locomotion during prey capture in centrarchid fishes. *J. Exp. Biol.* **210**, 107–117.

Higham, T. E., Malas, B., Jayne, B. C. and Lauder, G. V. (2005). Constraints on starting and stopping: behavior compensates for reduced pectoral fin area during braking of the bluegill sunfish *Lepomis macrochirus*. *J. Exp. Biol.* **208**, 4735–4746.

Holzman, R., Collar, D. C., Mehta, R. S. and Wainwright, P. C. (2011). An integrative modeling approach to elucidate suction-feeding performance. *J. Exp. Biol.* **215**, 1–13.

Howland, H. C. (1974). Optimal strategies for predator avoidance: The relative importance of speed and manoeuvrability. *J. Theor. Biol.* **47**, 333–350.

Humphries, D. A. and Driver, P. M. (1970). Protean defence by prey animals. *Oecologia* **5**, 285–302.

Isaacs, R. (1965). *Differential Games: A Mathematical Theory with Applications to Warfare and Pursuit, Control and Optimization*. New York: John Wiley and Sons, Inc.

Jarmark, B., Merz, A. W. and Breakwell, J. V. (1981). The variable-speed tail-chase aerial combat problem. *Journal of guidance* .

Justh, E. W. and Krishnaprasad, P. S. (2006). Steering laws for motion camouflage. *Proceedings of the Royal Society of London A: Mathematical, Physical and Engineering Sciences* **462**, 3629–3643.

Kane, E. A. and Higham, T. E. (2011). The integration of locomotion and prey capture in divergent cottid fishes: functional disparity despite morphological similarity. *J. Exp. Biol.* **214**, 1092–1099.

Kane, E. A. and Higham, T. E. (2014). Modelled three-dimensional suction accuracy predicts prey capture success in three species of centrarchid fishes. *J., Roy. Soc. Interface* **11**, 20140223.

Kane, S. A., Fulton, A. H. and Rosenthal, L. J. (2015). When hawks attack: animal-borne video studies of goshawk pursuit and prey-evasion strategies. *J. Exp. Biol.* **218**, 212–222.

Kane, S. A. and Zamani, M. (2014). Falcons pursue prey using visual motion cues: new perspectives from animal-borne cameras. *J. Exp. Biol.* **217**, 225–234.

Karaman, S. and Frazzoli, E. (2011a). Incremental Sampling-Based Algorithms for a Class of Pursuit-Evasion Games. In *Algorithmic Foundations of Robotics IX*, pp. 71–87. Berlin, Heidelberg: Springer Berlin Heidelberg.

Karaman, S. and Frazzoli, E. (2011b). Sampling-based algorithms for optimal motion planning. *International Journal of Robotics Research* **30**, 846–894.

Kram, R., Wong, B. and Full, R. (1997). Three-dimensional kinematics and limb kinetic energy of running cockraoches. *J. Exp. Biol.* **200**, 1919–1929.

Kullberg, C., Jakobsson, S. and Fransson, T. (1998). Predator-induced take-off strategy in great tits (Parus major). *Proceedings of the Royal Society of London. Series B: Biological Sciences* **265**, 1659–1664.

Land, M. F. and Collett, T. S. (1974). Chasing behaviour of houseflies (Fannia canicularis). *Journal of Comparative Physiology a-Sensory Neural and Behavioral Physiology* **89**, 331–357.

Lima, S. L. (2002). Putting predators back into behavioral predator-prey interactions. *Trends in Ecology & Evolution* **17**, 70–75.

Lima, S. L. and Dill, L. M. (2011). Behavioral decisions made under the risk of predation: a review and prospectus. *Canadian Journal of Zoology* **68**, 619–640.

Liu, K. and Fetcho, J. (1999). Laser ablations reveal functional relationships of segmental hindbrain neurons in zebrafish. *NEURON* **23**, 325–335.

Lucas, K. N., Dabiri, J. O. and Lauder, G. V. (2017). A pressure-based force and torque prediction technique for the study of fish-like swimming. *PLOS ONE* **12**, e0189225.

Martin-Fernandez, M. L., Tynan, C. J. and Webb, S. E. D. (2013). A 'pocket guide' to total internal reflection fluorescence. *J. Microscopy* **252**, 16–22.

McElroy, E. J., Meyers, J. J., Reilly, S. M. and Irschick, D. J. (2007). Dissecting the effects of behaviour and habitat on the locomotion of a lizard (Urosaurus ornatus). *Animal Behaviour* **73**, 359–365.

McHenry, M. J., Johansen, J. L., Soto, A. P., Free, B. A., Paley, D. A. and Liao, J. C. (2019). The pursuit strategy of predatory bluefish (Pomatomus saltatrix). *Proceedings. Biological sciences / The Royal Society* **286**, 20182934.

McHenry, M. J. and Lauder, G. (2005). The mechanical scaling of coasting in zebrafish (*Danio rerio*). *J. Exp. Biol.* **208**, 2289–2301.

McLean, D. L. and Fetcho, J. R. (2011). Movement, technology and discovery in the zebrafish. *Curr. Opin. Neurobiol.* **21**, 110–115.

Mead, K. S., Wiley, M. B., Koehl, M. A. R. and Koseff, J. R. (2003). Fine-scale patterns of odor encounter by the antennules of mantis shrimp tracking turbulent plumes in wave-affected and unidirectional flow. *J. Exp. Biol.* **206**, 181–193.

Merz, A. W. (1971). *Dissertation: The Homicidal Chauffeur – A Differential Game.* Stanford University.

Miller, L. A., Goldman, D. I., Hedrick, T. L., Tytell, E. D., Wang, Z. J., Yen, J. and Alben, S. (2012). Using Computational and Mechanical Models to Study Animal Locomotion. *Integr. Comp. Biol.* **52**, 553–575.

Mills, R., Hildenbrandt, H., Taylor, G. K. and Hemelrijk, C. K. (2018). Physics-based simulations of aerial attacks by peregrine falcons reveal that stooping at high speed maximizes catch success against agile prey. *PLoS Comp. Biol.* **14**, e1006044.

Mirat, O., Sternberg, J., Severi, K. and Wyart, C. (2013). Zebrazoom: an automated program for high-throughput behavioral analysis and categorization. *Front. Neur. Circ.* **7**, 107.

Mischiati, M., Lin, H.-T., Herold, P., Imler, E., Olberg, R. and Leonardo, A. (2015). Internal models direct dragonfly interception steering. *Nature* **517**, 333–338.

Miyawaki, A., Sawano, A. and Kogure, T. (2003). Lighting up cells: labelling proteins with fluorophores. *Nat. Cell Biol.* **5**, S1–S7.

Moore, T. Y. and Biewener, A. A. (2015). Outrun or Outmaneuver: Predator–Prey Interactions as a Model System for Integrating Biomechanical Studies in a Broader Ecological and Evolutionary Context. *Integr. Comp. Biol.* **55**, 1188–1197.

Morgansen, K. A., Duidam, V., Mason, R. J., Burdick, J. W. and Murray, R. M. (2001). Nonlinear control methods for planar carangiform robot fish locomotion. In *2001 ICRA. IEEE International Conference on Robotics and Automation*, pp. 427–434. IEEE.

Morgansen, K. A., Triplett, B. I. and Klein, D. J. (2007). Geometric Methods for Modeling and Control of Free-Swimming Fin-Actuated Underwater Vehicles. *IEEE Transactions on Robotics* **23**, 1184–1199.

Morice, S., Pincebourde, S., Darboux, F., Kaiser, W. and Casas, J. (2013). Predator-Prey Pursuit-Evasion Games in Structurally Complex Environments. *Integr. Comp. Biol.* **53**, 767–779.

Müller, U. K., Stamhuis, E. and Videler, J. J. (2000). Hydrodynamics of unsteady fish swimming and the effects of body size: Comparing the flow fields of fish larvae and adults. *J. Exp. Biol.* **203**, 193–206.

Müller, U. K. and van Leeuwen, J. L. (2004). Swimming of larval zebrafish: ontogeny of body waves and implications for locomotory development. *J. Exp. Biol* **207**, 853–868.

Nahin, P. J. (2007). *Chases and Escapes: The Mathematics of Pursuit and Evasion.* Princeton University Press.

Nikoueeyan, P. and Naughton, J. W. (2018). A photogrammetric approach for masking particle image velocimetry images around moving bodies. *Meas. Sci. Technol.* **29**, 105203.

Olberg, R. M., Seaman, R. C., Coats, M. I. and Henry, A. F. (2007). Eye movements and target fixation during dragonfly prey-interception flights. *Journal of Comparative Physiology A* **193**, 685–693.

Olberg, R. M., Worthington, A. H. and Venator, K. R. (2000). Prey pursuit and interception in dragonflies. *Journal of Comparative Physiology A* **186**, 155–162.

Paglianti, A. and Domenici, P. (2006). The effect of size on the timing of visually mediated escape behaviour in staghorn sculpin *Leptocottus armatus*. *J. Fish Biol.* **68**, 1177–1191.

Paoletti, P. and Mahadevan, L. (2014). Intermittent locomotion as an optimal control strategy. *Proceedings of the Royal Society of London A: Mathematical, Physical and Engineering Sciences* **470**, –20130535.

Parak, W. J., Pellegrino, T. and Plank, C. (2005). Labelling of cells with quantum dots. *Nanotechnology* **16**, R9–R25.

Parichy, D. M. (2015). The Natural History of Model Organisms: Advancing biology through a deeper understanding of zebrafish ecology and evolution. *eLife* **4**, 56.

Robie, A. A., Seagraves, K. M., Egnor, S. E. R. and Branson, K. (2017). Machine vision methods for analyzing social interactions. *J. Exp. Biol.* **220**, 25–34.

Roth, E., Sponberg, S. and Cowan, N. J. (2014). A comparative approach to closed-loop computation. *Current Opinion in Neurobiology* **25**, 54–62.

Ruxton, G. D., Sherratt, T. N. and Speed, M. (2004). *Avoiding Attack:The Evolutionary Ecology of Crypsis, Warning Signals and Mimicry*. Oxford: OUP Oxford.

Sane, S. P. and Dickinson, M. H. (2002). The aerodynamic effects of wing rotation and a revised quasi-steady model of flapping flight. *J. Exp. Biol.* **205**, 1087–1096.

Scaradozzi, D., Palmieri, G., Costa, D. and Pinelli, A. (2017). BCF swimming locomotion for autonomous underwater robots: a review and a novel solution to improve control and efficiency. *Ocean Engineering* **130**, 437–453.

Schaefer, P. L. and Ritzmann, R. E. (2001). Descending influences on escape behavior and motor pattern in the cockroach. *Devel. Neurobiol.* **49**, 9–28.

Shifferman, E. and Eilam, D. (2004). Movement and direction of movement of a simulated prey affect the success rate in barn owl *Tyto alba* attack. *J. Avian Biol.* **35**, 111–116.

Shneydor, N. A. (1998). *Missile Guidance and Pursuit*. Kinematics, Dynamics and Control. Elsevier.

Stamhuis, E. J., Videler, J. J., van Duren, L. A. and Müller, U. K. (2002). Applying digital particle image velocimetry to animal-generated flows: Traps, hurdles and cures in mapping steady and unsteady flows in Re regimes between 10^{-2} and 10^{5}. *Exp. Fluids* **33**, 801–813.

Stewart, W. J., Cardenas, G. S. and McHenry, M. J. (2013). Zebrafish larvae evade predators by sensing water flow. *J. Exp. Biol.* **216**, 388–398.

Stewart, W. J., Nair, A., Jiang, H. and McHenry, M. J. (2014). Prey fish escape by sensing the bow wave of a predator. *J. Exp. Biol.* **217**, 4328–4336.

Suebsaiprom, P. and Lin, C.-L. (2015). Maneuverability modeling and trajectory tracking for fish robot. *Control Engineering Practice* **45**, 22–36.

Thielicke, W. and Stamhuis, E. (2014). PIVlab – Towards User-friendly, Affordable and Accurate Digital Particle Image Velocimetry in MATLAB. *J. Open Res. Softw.* **2**, 1202.

Tytell, E. D., Holmes, P. and Cohen, A. H. (2011). Spikes alone do not behavior make: why neuroscience needs biomechanics. *Current Opinion in Neurobiology* **21**, 816–822.

Tytell, E. D. and Lauder, G. V. (2004). The hydrodynamics of eel swimming I. Wake structure. *J. Exp. Biol.* **207**, 1825–1841.

Vanhooydonck, B. and Van Damme, R. (2003). Relationships between locomotor performance, microhabitat use and antipredator behaviour in lacertid lizards. *Functional Ecology* **17**, 160–169.

Vasquez, R. A., Ebensperger, L. A. and Bozinovic, F. (2002). The influence of habitat on travel speed, intermittent locomotion, and vigilance in a diurnal rodent. *Behavioral Ecology* **13**, 182–187.

Venkatraman, S., Jin, X., Costa, R. M. and Carmena, J. M. (2010). Investigating neural correlates of behavior in freely behaving rodents using inertial sensors. *J. Neurophys.* **104**, 569–575.

Videler, J. J. (1981). Swimming Movements, Body Structure, and Propulsion in Cod (*Gadus morhua*. In *Vertebrate Locomotion* (ed. M. H. Day), pp. 1–27. London: Zoological Society of London.

Wainwright, P. C., Ferry-Graham, L., Waltzek, T. B., Carroll, A. M., Hulsey, C. D. and Grubich, J. R. (2001). Evaluating the use of ram and suction during prey capture by cichlid fishes. *J. Exp. Biol.* **204**, 3039–3051.

Walker, J. A., Ghalambor, C. K., Griset, O. L., McKenney, D. and Reznick, D. N. (2005). Do faster starts increase the probability of evading predators? *Functional Ecology* **19**, 808–815.

Wang, J., McKinley, P. K. and Tan, X. (2015). Dynamic Modeling of Robotic Fish With a Base-Actuated Flexible Tail. *Journal of Dynamic Systems Measurement and Control-Transactions of the Asme* **137**.

Watson, J. T. and Ritzmann, R. E. (1997). Leg kinematics and muscle activity during treadmill running in the cockroach. *J. Comp. Physiol. A* **182**, 11–22.

Webb, J. N. (2007). *Game Theory: Decisions, Interaction and Evolution.* London: Springer.

Weihs, D. (1973). The mechanism of rapid starting of slender fish. *Biorheology* **10**, 343–350.

Weihs, D. and Webb, P. W. (1984). Optimal avoidance and evasion tactics in predator-prey interactions. *J. Theor. Biol.* **106**, 189–206.

Wilson, A. M., Lowe, J. C., Roskilly, K., Hudson, P. E., Golabek, K. A. and McNutt, J. W. (2013). Locomotion dynamics of hunting in wild cheetahs. *Nature* **498**, 185–189.

Yuan, L. C. L. (1948). Homing and Navigational Courses of Automatic Target-Seeking Devices. *J. Applied Physics* **19**, 1122–1128.

Appendix A

Chapter 1 Supplemental Material

A.1 Performance plateau in the slow-predator domain

The present study included the results of numerical solutions that showed a performance plateau in the slow-predator domain, where the prey is faster than the predator. Here we define the boundary to this plateau, where an equivalent escape performance is achieved for a large range of escape angles α (Fig. 2A). For each escape angle in this range, the prey performs equally well by not allowing the predator to approach any closer than the distance at which the prey initiates an escape.

The distance between predator and prey varies with time, as given by the following equation:

$$D^2 = ((X_0 - Ut) + Vt\cos\alpha)^2 + (Vt\sin\alpha)^2, \tag{A.1}$$

where U and V are respectively the predator and prey speeds that do not vary with time, and X_0 is the initial position of the prey (i.e. $D^2 = X_0^2$ at $t = 0$). As explained in our article, the distance function may be solved for the time at which the minimum distance

between predator and prey is achieved. The minimum distance distance occurs at $t = 0$ if the distance function increases monotonically with time. All escape angles for which this is true will yield an ideal minimum distance ($\frac{D}{X_0} = 1$). We will consider whether this is true of the following range of angles, which is bounded by the two solutions to Eqn. A.1 reported by Weihs and Webb (1984):

$$0 \leq \alpha \leq \arccos(K), \tag{A.2}$$

where $K = U/V$. For our purposes, it is helpful to formulate this inequality as follows:

$$K \leq \cos\alpha \leq 1. \tag{A.3}$$

Toward this aim, it suffices to show that the distance function is increasing for all positive time values. This may be achieved by proving that the derivative of Eqn. A.1 with respect to time is greater than or equal to zero. This derivative is given by the following equation:

$$\frac{\partial D^2}{\partial t} = 2(t(U^2 + V^2) - UX_0 + V(X_0 - 2tU)\cos\alpha). \tag{A.4}$$

It is helpful to rewrite this expression as a linear function of time as follows:

$$\frac{\partial D^2}{\partial t} = 2(U^2 + V^2 - 2UV\cos\alpha)t + 2X_0(V\cos\alpha - U), \tag{A.5}$$

In order to show that Eqn. A.5 is nonnegative for $t \geq 0$, it suffices to show that the slope is positive and the intercept (when $t = 0$) is nonnegative.

- Positive slope.

  Eqn. A.3 implies that $V\cos\alpha \leq V$. Multiplying this inequality by $-2U$ and adding

$U^2 + V^2$ on both sides yields:

$$U^2 + V^2 - 2UV\cos\alpha \geq V^2 - 2UV + U^2 \tag{A.6}$$

The right hand side of this inequality is equivalent to $(V - U)^2$. Because $K < 1$, it follows that $V > U$. Thus,

$$U^2 + V^2 - 2UV\cos\alpha \geq (V - U)^2 > 0 \tag{A.7}$$

- Nonnegative intercept.

  Because we consider only the situation where $X_0 > 0$, we simply need to show that $V\cos\alpha - U \geq 0$.

  Eqn. A.3 implies that $KV \leq V\cos\alpha$. Since $K = U/V$, we have

$$U \leq V\cos\alpha. \tag{A.8}$$

  We can rewrite this inequality as

$$V\cos\alpha - U \geq 0. \tag{A.9}$$

Eqns. A.6 and A.9 together show that the distance is always increasing for $0 \leq \alpha \leq \arccos(K)$ and $K < 1$. An analogous argument applies for $-\arccos(K) \leq \alpha < 0$. The preceding proof shows that the minimum distance occurs at $t = 0$ and is given by $D^2 = X_0^2$. This defines a performance plateau for the prey as a wide range of angles that yield equally successful escapes.

A.2 Initial Lateral Displacement

The distance function given by Eqn. A.1 is based on the assumption that the predator is headed directly at the initial position of the prey. However, previous experiments have shown that predators often fail to perfectly align their approach toward the prey. To model this situation, here we introduce a lateral initial position to the distance function.

A.2.1 Distance function with initial lateral displacement

This general form of the distance function is now given by the following:

$$D^2 = ((X_0 - Ut) + Vt\cos\alpha)^2 + (Y_0 + Vt\sin\alpha)^2. \tag{A.10}$$

Note that the introduction of an initial lateral position (Y_0) allows us to rewrite the equation in polar coordinates, which simplifies our analysis below. We can rewrite Eqn. A.10 in polar coordinates (R, θ) by setting $R_0^2 = X_0^2 + Y_0^2$, and $\theta_0 = \arctan(Y_0/X_0)$. Here we assume that $Y_0 \geq 0$, but the final results are presented for the more general case. This yields the following:

$$D_0^2 = R_0^2 + (1 + K^2)t^2V^2 - 2Vt(KVt\cos\alpha - R_0\cos(\alpha - \theta_0) + KR_0\cos\theta_0). \tag{A.11}$$

To find the time at which Eqn. A.11 is minimal, we find the roots of the derivative of Eqn. A.11 with respect to t, which yields the following solution:

$$t_{\min} = \frac{R_0}{V}\frac{[K\cos\theta_0 - \cos(\alpha - \theta_0)]}{1 - 2K\cos\alpha + K^2} \tag{A.12}$$

The above is negative when $K\cos\theta_0 < \cos(\alpha-\theta_0)$. Rewriting this inequality gives the range of α for which the distance is solely increasing. Explicitly, this is given by the following:

$$\theta_0 - \arccos(K\cos\theta_0) < \alpha < \theta_0 + \arccos(K\cos\theta_0). \tag{A.13}$$

For these values of α, the minimum distance occurs at $t = 0$ and is thus equal to the initial distance R_0^2. This defines a performance plateau when $K < 1$. If we now substitute $t_{\min}$ for t in Eqn. A.11, we get the minimum distance as a function of α with respect to parameters K and θ_0. This is given by the following:

$$\overline{D}^2_{\min} = \frac{D^2_{\min}}{R_0^2} = \frac{(\sin(\alpha-\theta_0) + K\sin\theta_0)^2}{K^2 - 2K\cos\alpha + 1}. \tag{A.14}$$

A.2.2 Finding values of α that optimize the minimum distance

To find the escape angle which yields the largest minimum distance, we solved the following equation:

$$0 = \frac{\partial \overline{D}^2_{\min}}{\partial\alpha} = \frac{2(K\cos\alpha - 1)(K\cos\theta_0 - \cos(\alpha-\theta_0))(K\sin\theta_0 + \sin(\alpha-\theta_0))}{(K^2 - 2K\cos\alpha + 1)^2} \tag{A.15}$$

The solutions to this equation are found by finding where the numerator is equal to zero which is done by considering the following three cases:

Case 1: $K\cos\alpha - 1 = 0$.

Solving this equation yields the following relationship:

$$\alpha_1 = \pm\arccos K^{-1} \tag{A.16}$$

This solution is valid for $K \geq 1$, which indicates that prey are equally effective if escaping at an optimal angle toward the left ($\alpha > 0$), or right ($\alpha < 0$) of the predator's heading.

Case 2: $K\cos\theta_0 - \cos(\alpha - \theta_0) = 0$.

A careful analysis is required for this case because the solution can include complex numbers for some combinations of K and θ_0. This equation may be formulated as follows:

$$\cos(\alpha - \theta_0) = K\cos\theta_0. \tag{A.17}$$

This equation imposes conditions on the values of K and θ_0 to yield solutions which are real numbers. Explicitly, this condition is given by the following

$$|K\cos\theta_0| \leq 1 \tag{A.18}$$

Eqn. A.18 is always satisfied when $0 \leq K \leq 1$. If $K > 1$, then we must have that $|\cos\theta_0| \leq 1/K$. This leads to the following bound for θ_0:

$$\arccos(K^{-1}) \leq \theta_0 \leq \arccos(-K^{-1}). \tag{A.19}$$

Note that as the value of K increases, the allowable range for θ_0 decreases. With these restrictions in mind, we proceed to solve Eqn. A.17. The solution is given by:

$$\alpha_2 = \theta_0 + \arccos(K\cos\theta_0),$$
$$\alpha_3 = \theta_0 - \arccos(K\cos\theta_0).$$

Therefore, the following equation defines the boundaries of the performance plateau for $K < 1$:

$$|\alpha - \theta_0| \leq \arccos(K\cos\theta_0). \tag{A.20}$$

For $K > 1$, the solutions $\alpha_{2,3}$ are not optimal unless θ_0 simultaneously satisfies Eqn. A.19.

Case 3: $K \sin\theta_0 + \sin(\alpha - \theta_0) = 0$.

Solving this equation yields the following:

$$\alpha_4 = \theta_0 - \arcsin(K \sin\theta_0),$$
$$\alpha_5 = \pi + \theta_0 + \arcsin(K \sin\theta_0).$$

For $K < 1$, α_4 is contained within the bounds defined by Eqn. A.13. This means that the solution is contained within the performance plateau of the slow–predator domain. When $K > 1$, α_4 is a local minimum. Because we seek to find the angle which yields the greatest minimum distance, α_4 is not optimal when $K > 1$. Similarly, the solution given by α_5 is a local minimum for all values of K, so this solution does not yield an optimal escape.